Article

Developmental Cell

Fat2 and Lar Define a Basally Localized Planar Signaling System Controlling Collective Cell Migration

Highlights

- Fat2 and Lar localize to juxtaposing membrane domains and promote tissue motility
- Fat2 signals from the trailing edge to induce protrusions in the cell behind
- Fat2 stabilizes Lar's localization at the leading edge of the cell behind
- Lar signals from the leading edge to promote rear retraction in the cell ahead

Authors

Kari Barlan, Maureen Cetera, Sally Horne-Badovinac

Correspondence

shorne@uchicago.edu

In Brief

Barlan and colleagues examine how the cadherin Fat2 and the receptor tyrosine phosphatase Lar promote epithelial migration in the context of the *Drosophila* egg chamber. They show that these proteins form the core of a planar signaling system that coordinates leading and trailing edge dynamics between neighboring cells.

Barlan et al., 2017, Developmental Cell *40*, 467–477
March 13, 2017
http://dx.doi.org/10.1016/j.devcel.2017.02.003

CellPress

Developmental Cell
Article

Fat2 and Lar Define a Basally Localized Planar Signaling System Controlling Collective Cell Migration

Kari Barlan,[1] Maureen Cetera,[2,3] and Sally Horne-Badovinac[1,2,4,*]
[1]Department of Molecular Genetics and Cell Biology
[2]Committee on Development, Regeneration and Stem Cell Biology
The University of Chicago, 920 East 58th Street, Chicago, IL 60637, USA
[3]Present address: Department of Molecular Biology, Princeton University, 247 Lewis Thomas Laboratory, Washington Road, Princeton, NJ 08544, USA
[4]Lead Contact
*Correspondence: shorne@uchicago.edu
http://dx.doi.org/10.1016/j.devcel.2017.02.003

SUMMARY

Collective migration of epithelial cells underlies diverse tissue-remodeling events, but the mechanisms that coordinate individual cell migratory behaviors for collective movement are largely unknown. Studying the *Drosophila* follicular epithelium, we show that the cadherin Fat2 and the receptor tyrosine phosphatase Lar function in a planar signaling system that coordinates leading and trailing edge dynamics between neighboring cells. Fat2 signals from each cell's trailing edge to induce leading edge protrusions in the cell behind, in part by stabilizing Lar's localization in these cells. Conversely, Lar signals from each cell's leading edge to stimulate trailing edge retraction in the cell ahead. Fat2/Lar signaling is similar to planar cell polarity signaling in terms of sub-cellular protein localization; however, Fat2/Lar signaling mediates short-range communication between neighboring cells instead of transmitting long-range information across a tissue. This work defines a key mechanism promoting epithelial migration and establishes a different paradigm for planar cell-cell signaling.

INTRODUCTION

Collective migration of cells within an epithelial sheet underlies tissue-remodeling events associated with morphogenesis, wound repair, and the metastatic cascade (Friedl and Gilmour, 2009; Mayor and Etienne-Manneville, 2016; Pocha and Montell, 2014). Similar to individually migrating cells, each epithelial cell extends actin-rich protrusions at its leading edge that form new adhesions to the extracellular matrix (ECM). Each cell also releases these adhesions at its rear to allow the trailing edge to retract and cell body to advance. Unlike individually migrating cells, however, migrating epithelial cells must coordinate these behaviors with their neighbors. Most epithelial cells' leading edge protrusions extend beneath the trailing edges of the cells ahead, similar to overlapping shingles on a roof (Figures 1A and 1B). Hence, trailing edge retraction in the leading cell must be tightly coordinated with protrusion formation in the trailing cell. How this local cell-cell coordination is achieved is unknown.

One way that leading and trailing edge dynamics could be coordinated between migrating epithelial cells is through the use of a planar signaling system. In these systems, distinct sets of transmembrane proteins localize to opposite sides of the same cell and then mediate intercellular communication by interacting with one another across cell-cell boundaries. However, the well-known Frizzled/Van Gogh (Fz/Vang) and Fat/Dachsous (Ft/Ds) planar cell polarity (PCP) pathways that organize many epithelia operate near the apical surface (Devenport, 2014; Matis and Axelrod, 2013), whereas the cell migration machinery is at the basal surface. These distinct localizations make it unlikely that known PCP systems coordinate individual cell migratory behaviors at the basal surface.

The *Drosophila* egg chamber provides a powerful model to investigate the mechanisms controlling epithelial migration (Figures 1C–1G). Egg chambers are multicellular assemblies within the ovary that each produces one egg. They have a germ cell cluster that is surrounded by a somatic epithelium called the follicle cells. The basal epithelial surface contacts a basement membrane ECM that ensheaths the egg chamber. From the time an egg chamber forms until stage 8 of oogenesis, the follicle cells collectively migrate along their basement membrane (Cetera et al., 2014; Chen et al., 2016; Haigo and Bilder, 2011). This migration causes the egg chamber to rotate within its surrounding ECM, which remains stationary (Haigo and Bilder, 2011). There is strong evidence that this rotational motion helps to transform the egg chamber from a spherical to an ellipsoidal shape (Cetera et al., 2014; Haigo and Bilder, 2011; Isabella and Horne-Badovinac, 2016); however, one instance has been reported in which rotation and elongation appear to be decoupled (Aurich and Dahmann, 2016).

The Fz/Vang and Ft/Ds PCP pathways are not required for the migration of the follicular epithelium (Viktorinova et al., 2009). However, previous work identified two transmembrane proteins that are excellent candidates to mediate planar signaling at the basal surface and thus promote migration of this tissue: the

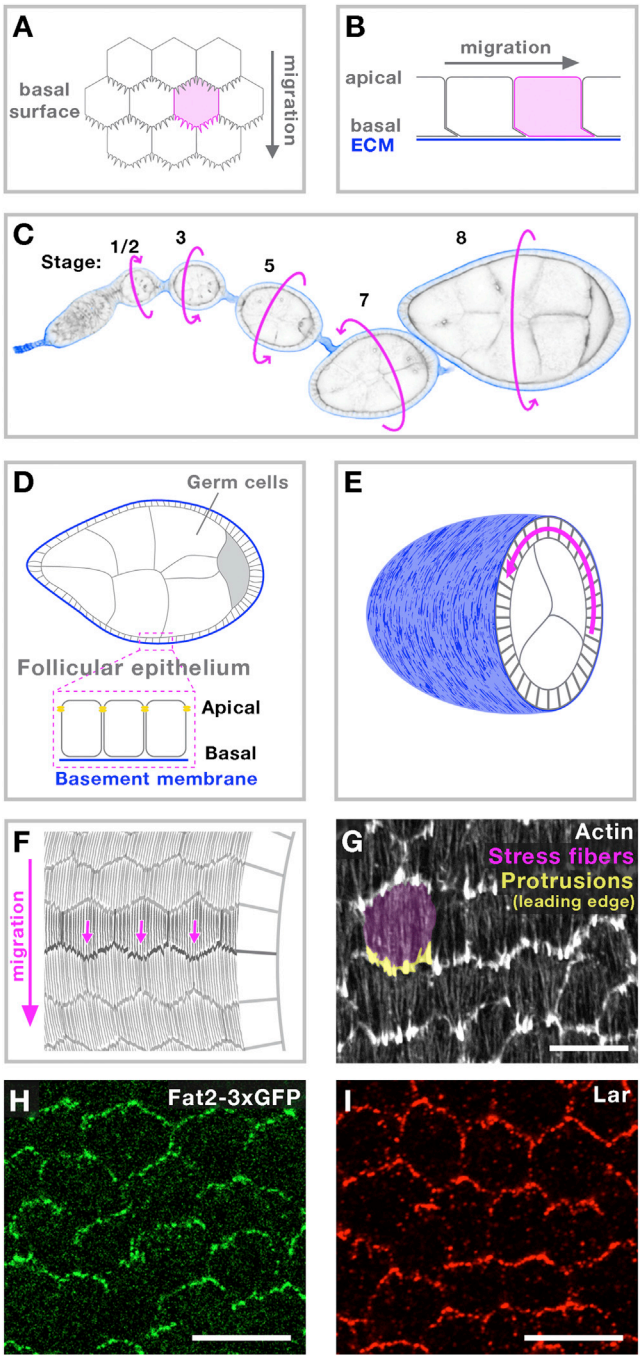

Figure 1. The Developmental Context for the Migration of the Follicular Epithelium

(A and B) Illustrations showing a migrating epithelium from basal (A) and side (B) views. Protrusion size has been exaggerated in (B) to increase visibility.

(C) Micrograph of a developmental array of egg chambers, highlighting the period when rotation (arrows) occurs.

(D) Illustration of a central sagittal section through an egg chamber.

(E) Illustration of a central transverse section through an egg chamber. During their migration (arrow), the follicular epithelial cells crawl along the basement membrane, which remains stationary.

(F) Illustration of the basal surface of the follicular epithelium. During migration, the actin cytoskeleton is planar polarized, with stress fibers oriented in the direction of movement and leading edge protrusions oriented orthogonally (arrows).

(G) Micrograph of actin-based structures at the basal surface of the follicular epithelium at stage 7. A single cell is highlighted. The direction of migration is down, as determined by the orientation of leading edge protrusions.

(H and I) Micrographs showing planar polarization of Fat2-3xGFP (H) and Lar (I) at the basal surface at stage 7.

Scale bars, 10 μm.

atypical cadherin Fat2 and the receptor tyrosine phosphatase leukocyte antigen related (Lar) (Bateman et al., 2001; Frydman and Spradling, 2001; Gutzeit et al., 1991; Viktorinova et al., 2009). Fat2 (also known as Kugelei) shows a planar polarized distribution at the basal surface, such that it is present on cell-cell interfaces roughly perpendicular to the direction of tissue motility, and is absent from the lateral cell-cell interfaces (Viktorinova et al., 2009) (Figure 1H). It was later shown that this localization corresponds to each cell's trailing edge and that Fat2 is required for collective follicle cell migration (Cetera et al., 2014; Chen et al., 2016; Viktorinová and Dahmann, 2013). A recent model proposed that Fat2 promotes epithelial motility by stimulating the formation of leading edge protrusions on a cell-autonomous basis (Squarr et al., 2016); however, how this model fits with Fat2's trailing edge localization is unclear. Lar is planar polarized at the basal epithelial surface similar to Fat2 (Bateman et al., 2001) (Figure 1I), and Lar has also been proposed to stimulate the formation of leading edge protrusions on a cell-autonomous basis (Squarr et al., 2016). However, Lar's sub-cellular localization (i.e., leading edge versus trailing edge) and role in epithelial motility are less well defined. Whether Fat2 and Lar work together to control the formation of leading edge protrusions is also unknown.

Here we show that Fat2 and Lar participate in a planar signaling system that coordinates leading and trailing edge dynamics between migrating epithelial cells. First we show that Lar's planar polarized distribution corresponds to each cell's leading edge and that Lar is required for epithelial migration. We then show that, contrary to the current model, Fat2's role in protrusion formation is non-cell-autonomous. Specifically, Fat2 signals from the trailing edge of each cell to induce the formation of leading edge protrusions in the cell directly behind, in part by stabilizing Lar at the leading edge of this cell. Finally, we introduce a role for Fat2 and Lar in the control of trailing edge retraction by showing that Lar signals from the leading edge of each cell to stimulate the retraction in the cell directly ahead and that Fat2 plays a cell-autonomous role in this process. Altogether, this work defines a key mechanism driving epithelial migration and establishes a new paradigm for planar cell-cell signaling.

RESULTS

Lar Promotes Epithelial Migration and Localizes to Each Cell's Leading Edge

To investigate whether Fat2 and Lar participate in a planar signaling system controlling epithelial migration, we first needed to better define Lar's role in this process. Live imaging revealed that *Lar* null epithelia show a fully penetrant yet variable defect in their motility (Figures 2A–2D and S1A–S1C, Table S1, and Movie S1). We defined a *Lar* epithelium as being "non-migratory" if it had a migration rate that was less than that of the fastest rate obtained for a *fat2* null epithelium in the same experiment (i.e.,

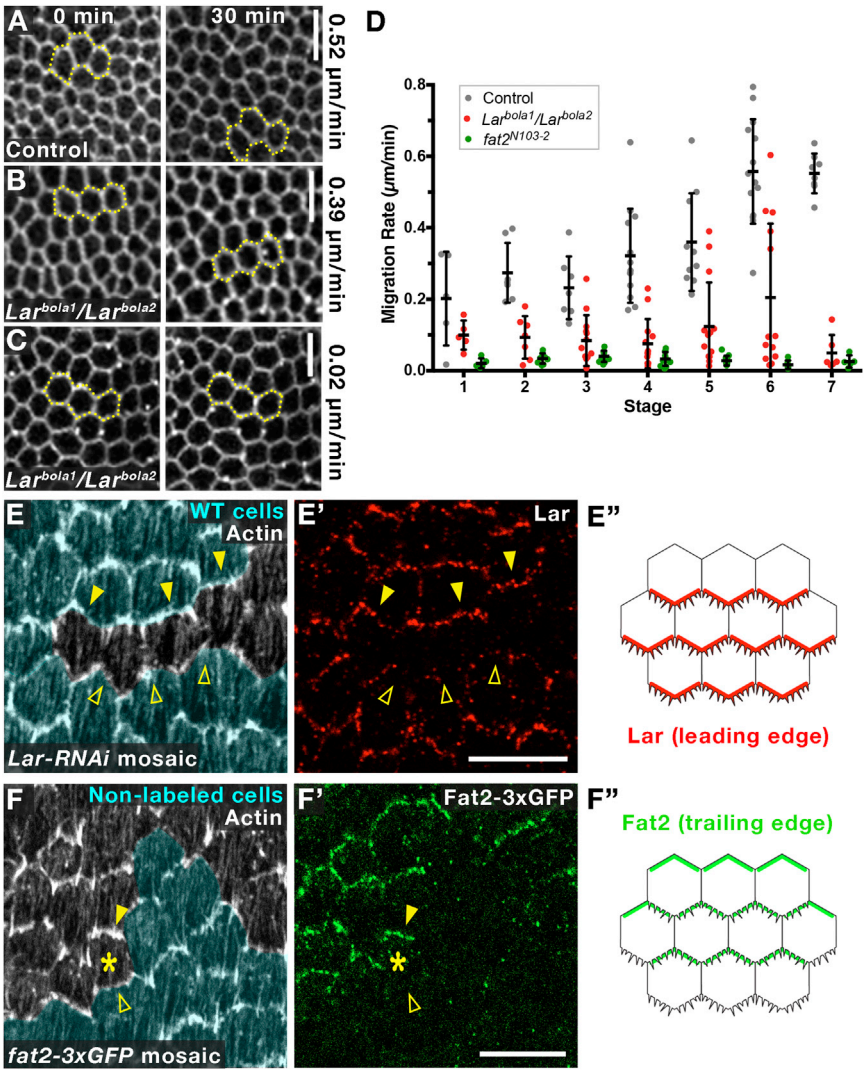

Figure 2. Lar and Fat2 Promote Follicle Cell Migration and Localize to Juxtaposing Cell Edges at the Basal Epithelial Surface

(A–C) Still images from time-lapse movies of control (A), Lar^{bola1}/Lar^{bola2} (B), and (C) stage 6 epithelia. Dotted lines mark the same three cells across each time series. Some Lar^{bola1}/Lar^{bola2} epithelia migrate slowly (B) while some do not migrate (C). Scale bars, 10 μm.

(D) Migration rates for control, Lar^{bola1}/Lar^{bola2}, and $fat2^{N103-2}$ epithelia. Individual data points, mean ± SD. See Table S1 for sample sizes and p values.

(E and E′) Mosaic expression of *Lar-RNAi*. Wild-type cells are pseudocolored cyan. Lar is enriched at the leading edge of wild-type cells behind the clone (solid triangles), compared with the trailing edge of wild-type cells ahead of the clone (open triangles). Scale bar, 10 μm.

(F and F′) Mosaic epithelium showing Fat2-3xGFP's sub-cellular localization. Cells not expressing *fat2-3xGFP* are pseudocolored cyan. Asterisk marks one cell. Fat2-3xGFP is present at the cell's trailing edge (solid triangle) but not at the leading edge (open triangle). Scale bar, 10 μm.

(E and F) Stage 7 epithelia and the direction of migration is down.

(E″ and F″) These illustrations depict Lar and Fat2 distributions at the basal surface.

See also Figures S1, S2, Table S1, and Movie S1.

0.067 μm/min), as *fat2* epithelia have been established to never migrate (Cetera et al., 2014; Chen et al., 2016). Using this metric, 48% of *Lar* null epithelia are non-migratory, whereas the rest migrate slower than controls. We then used mosaic analysis to map Lar's sub-cellular localization (Figure S1D). Analyzing Lar localization around clones of cells expressing *Lar-RNAi* revealed that Lar primarily localizes to each cell's leading edge (Figure 2E). Together, these data show that Lar promotes epithelial migration and that it likely does so by acting at the leading edge of each cell.

Fat2 and Lar Show a Planar Polarized Distribution throughout the Migratory Period

When combined with previous work on Fat2 (Viktorinová and Dahmann, 2013), the data above establish a framework wherein Fat2 and Lar act as pro-migratory proteins that localize to juxtaposing membrane domains, with Fat2 at the trailing edge of one cell and Lar at the leading edge of the cell behind. If this complementary localization pattern is important for epithelial motility, Fat2 and Lar should exhibit planar polarized distributions throughout the migratory period. It has been reported, however, that Fat2 and Lar exclusively localize to tricellular junctions during early migratory stages, and do not become planar polarized along cell membranes until stage 6 (Bateman et al., 2001; Viktorinova et al., 2009).

To visualize Fat2's and Lar's localizations in young egg chambers with more clarity, we used the CRISPR-Cas9 system to insert three copies of *GFP* into the *fat2* locus (*fat2-3xGFP*), creating a bright, functional protein fusion (Figures S2A–S2C), and confirmed that the Fat2-3xGFP protein localizes to each cell's trailing edge (Figure 2F). We also developed better immunostaining conditions for Lar (see STAR Methods). With these improved methods, we see Fat2 and Lar planar polarized along cell membranes from the very earliest stages of epithelial migration (Figures S2D and S2E). These data suggest that Fat2's and Lar's planar polarized localizations are likely to be integral to the migration process.

Fat2 and Lar Play Complementary Roles in the Formation of Leading Edge Protrusions

Fat2 and Lar have been proposed to promote epithelial migration by stimulating the formation of leading edge protrusions on a cell-autonomous basis (Squarr et al., 2016). This model fits well with Lar's localization along leading plasma membranes, but it is at odds with Fat2's localization along trailing plasma membranes. To explore this paradox, we analyzed leading edge protrusion formation in *Lar* and *fat2* mosaic

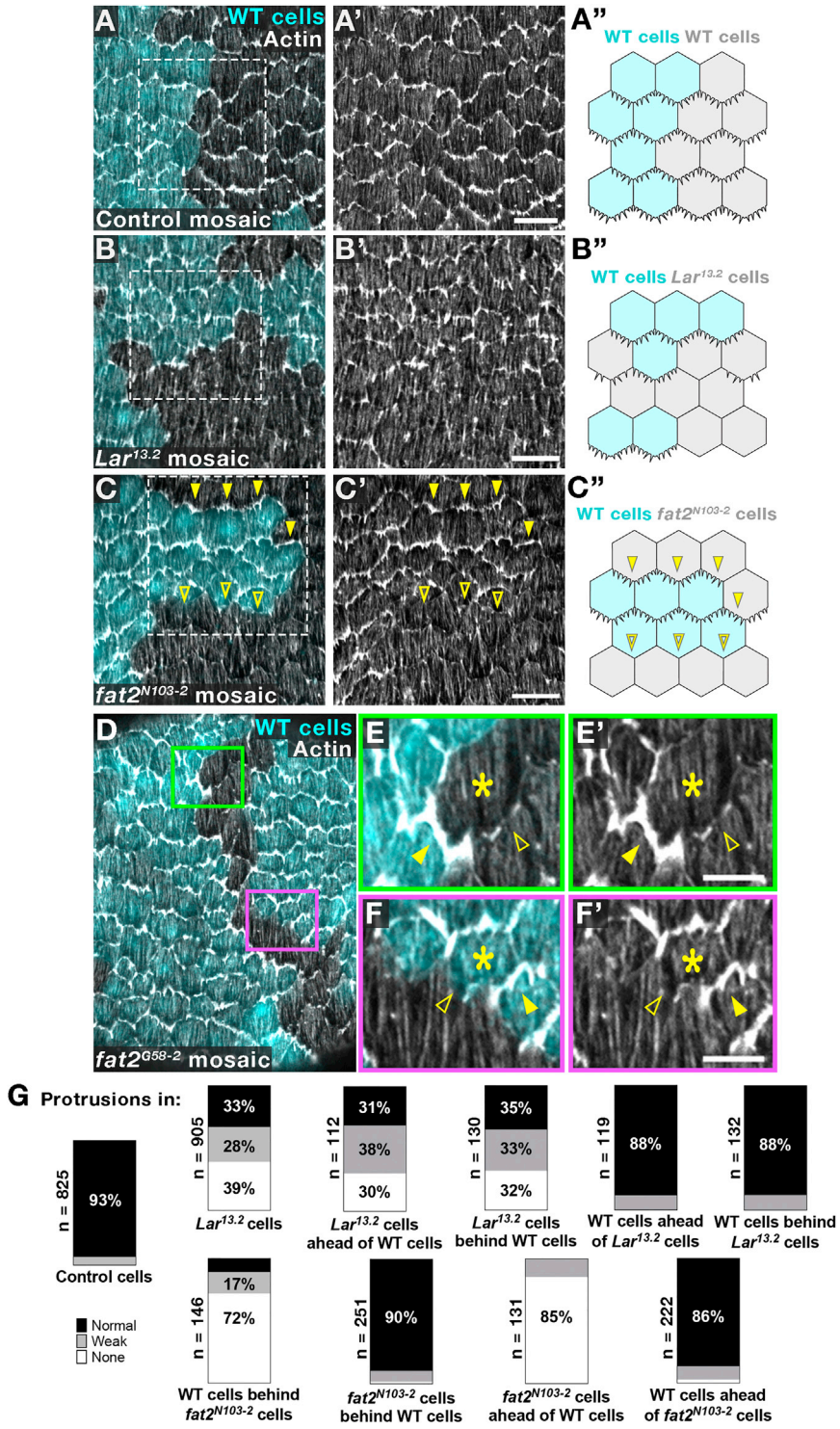

Figure 3. Fat2 and Lar Play Complementary Roles in Leading Edge Protrusion Formation

(A–C) Representative images of protrusion formation at the basal surface of control (A), $Lar^{13.2}$ (B), and $fat2^{N103-2}$ (C) mosaic epithelia. Protrusions are reduced within $Lar^{13.2}$ clones (B), (B′), while Fat2 functions non-cell-autonomously in protrusion formation (C), (C′). Wild-type cells directly behind $fat2^{N103-2}$ cells lack protrusions (open triangles); $fat2^{N103-2}$ cells directly behind wild-type cells form protrusions (solid triangles). Scale bars, 10 μm. Illustrations (A″), (B″), and (C″) depict results shown in boxed regions in micrographs.

(D–F) Basal surface of a $fat2^{G58-2}$ mosaic epithelium. (E) and (E′) Zoom of green boxed region in (D). The asterisk marks a $fat2^{G58-2}$ cell the leading edge of which contacts both a wild-type cell and a $fat2^{G58-2}$ cell. The portion of the leading edge that contacts the wild-type cell forms protrusions (solid triangle), whereas the portion that contacts the $fat2^{G58-2}$ cell does not (open triangle). (F) and (F′) Zoom of magenta boxed region in (D) showing that the same property holds true for a wild-type cell (asterisk). Scale bars, 5 μm (E′) and (F′).

(G) Quantification of protrusion formation in mosaic epithelia. Protrusions were scored by eye as either normal, weak, or absent (none). For *Lar* and *fat2* mosaic epithelia, this analysis was performed on the first row of cells just inside the clone and on the first row of cells just outside the clone, at both the leading and trailing boundaries of the clone.

Experiments performed at stage 7. Images oriented with direction of migration down.

See also Figure S1.

epithelia (Figures 3A–3G and S1E), as this is the only definitive way to determine the cell-autonomous versus non-cell-autonomous function of a pro-migratory signaling protein. These experiments confirmed Lar's cell-autonomous role in this process (Figures 3B and 3G), although protrusions are not entirely absent in *Lar* null clones. By contrast, we found that Fat2's role in protrusion formation is both strong and non-cell-autonomous (Figures 3C–3G). Specifically, wild-type cells positioned directly behind *fat2* null cells lack protrusions, whereas *fat2* cells positioned directly behind wild-type cells form protrusions normally. This non-cell-autonomous phenotype extends across only one cell-cell boundary. Further, when a cell's leading edge contacts both a *fat2* null cell and a wild-type cell, protrusions are lost only from the region contacting the *fat2* cell (Figures 3D–3F), which indicates that Fat2 signaling controls protrusion formation on a sub-cellular level. Thus, Fat2 signals from each cell's trailing edge to induce leading edge protrusions in the cells directly behind in a highly localized manner, whereas Lar plays a cell-autonomous role in this process.

Fat2 Stabilizes Lar in the Leading Plasma Membrane of Neighboring Cells

Given their complementary localization patterns and complementary roles in protrusion formation, we reasoned that Fat2

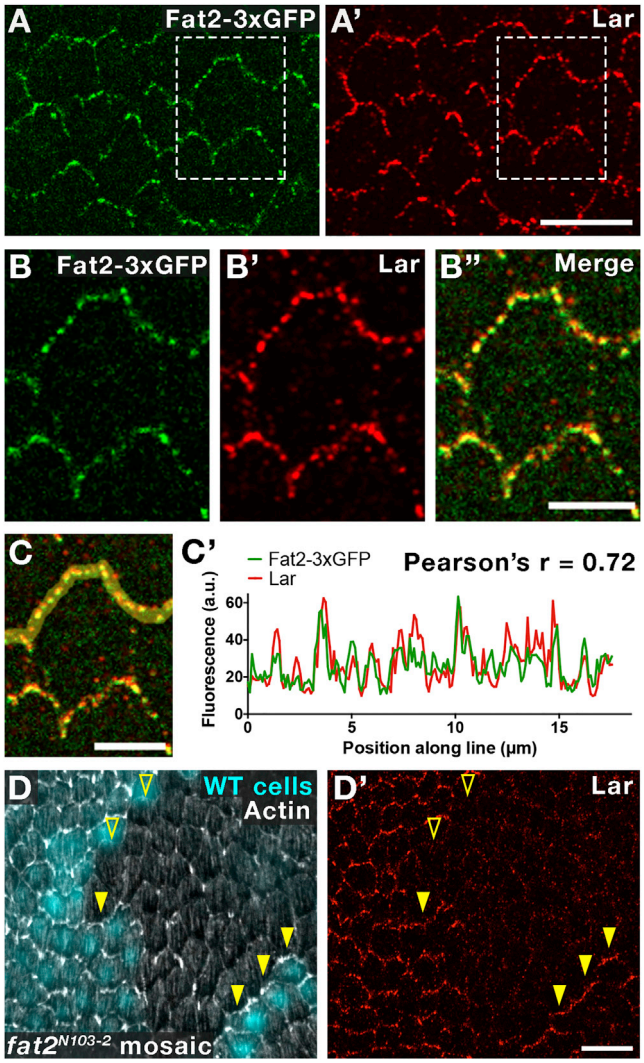

Figure 4. Fat2 Non-Cell-Autonomously Stabilizes Lar in Neighboring Cells

(A–C) Fat2-3xGFP and Lar puncta colocalize along cell-cell interfaces at the basal surface. Boxed regions in (A) and (A′) are blown up in (B) and (B′). (C) and (C′) Line-scan analysis on image data in (B). (C′) Fluorescence intensities and corresponding Pearson's coefficient for Fat2-3xGFP and Lar along the yellow line in (C). Scale bars, 10 μm (A), and 5 μm (B) and (C).

(D) Fat2 stabilizes Lar's localization in neighboring cells. Lar is absent from the leading edge of wild-type cells directly behind *fat2*$^{N103-2}$ cells (open triangles), but localizes normally in *fat2*$^{N103-2}$ cells directly behind wild-type cells (solid triangles). Scale bar, 10 μm.

See also Figure S3.

and Lar might control protrusive activity by functioning in a planar signaling pathway that mediates communication between neighboring cells. Fz/Vang and Ft/Ds PCP signaling complexes form distinct puncta along cell-cell interfaces near the apical epithelial surface (Hale et al., 2015; Strutt et al., 2011). We found that Fat2 and Lar colocalize in similar puncta along basal cell-cell interfaces (Figures 4A–4C). Performing line-scan analyses along these regions revealed that the correlation between Fat2 and Lar fluorescence is robust, with an average Pearson coefficient of 0.78 ± 0.06 (Figures 4C, S3A, and S3B). These data open the possibility that Fat2 and Lar participate in a signaling complex spanning cell-cell boundaries.

Given their striking colocalization, we next asked whether Fat2 and Lar are required for each other's localization. This question has been explored previously (Viktorinova et al., 2009), but the original experiments were performed on entirely mutant epithelia instead of mosaic epithelia, making it difficult to assess whether protein levels were altered in mutant cells compared with wild-type cells, and whether the phenotype was cell-autonomous or non-cell-autonomous. Moreover, because the earlier study was performed prior to the discovery of egg chamber rotation (Haigo and Bilder, 2011), the authors were unable to distinguish whether mislocalization of a given protein was due to loss of the other protein from the epithelium, per se, or to the loss of tissue motility. Therefore, we revisited this question taking these important variables into account.

Using mosaic epithelia, we discovered that Lar levels are significantly reduced at the basal surface of *fat2* null clones (Figure 4D). Careful examination of clone boundaries further revealed that this effect is non-cell-autonomous. Cells positioned directly behind *fat2* cells lack Lar at their leading edges, whereas *fat2* cells positioned directly behind wild-type cells retain Lar at their leading edges. This phenotype is not due to an effect on *Lar* expression, as Lar protein levels are normal at the apical surface of *fat2* clones (Figures S3C and S3D). Nor is it due to loss of protrusions behind *fat2* cells, as Lar still localizes normally in clones of cells expressing an RNAi transgene against the Wave regulatory complex (WRC) component Abelson interacting protein (Abi) (Figure S3E), which is required cell-autonomously for protrusion formation in the follicle cells (Cetera et al., 2014). By contrast, Fat2 levels and localization are more weakly affected in *Lar* null clones, and the defects that do occur are variable (Figures S3G–S3I). Altogether, these data suggest that Fat2 at the trailing edge of one cell stabilizes Lar's localization at the leading edge of the cell directly behind, but that Lar plays a less important role in localizing Fat2.

Our finding that Fat2 localization is only weakly affected in *Lar* null clones conflicts with the previous report that Fat2 is uniformly localized around basal cell edges in epithelia entirely mutant for *Lar* (Viktorinova et al., 2009). The difference in Fat2 localization between these studies may result from a difference in the ability of an entirely mutant versus a mosaic epithelium to migrate. Tissue migration can still occur in epithelia containing small clones of non-migratory cells, as the mutant cells are passively carried along by their wild-type neighbors (Cetera et al., 2014; Viktorinová and Dahmann, 2013), whereas tissue migration fails in epithelia entirely comprised of non-migratory cells. To explore this possibility, we examined Fat2 and Lar localization in epithelia where migration was blocked by loss of the WRC (Cetera et al., 2014), and found that Fat2 and Lar both lose their planar polarization (Figures 5A–5D). The two proteins do still colocalize in puncta at cell-cell interfaces under these conditions, however (Figure 5B). By contrast, Fat2 and Lar localize normally in clones lacking WRC function that can be carried along the migration path by their wild-type neighbors (Figures S3E and S3F). These data suggest that the Fat2 localization defect seen in *Lar* null epithelia (Viktorinova et al., 2009) may be secondary to the defect in tissue motility. They further indicate

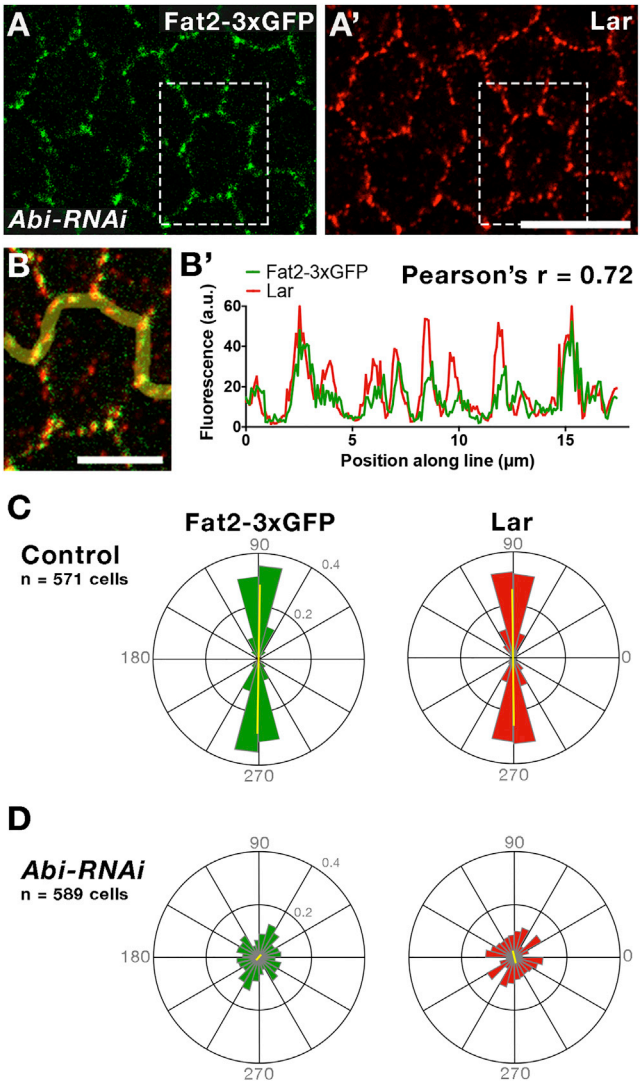

Figure 5. Epithelial Migration Is Required for Fat2's and Lar's Planar Polarization

(A and B) Representative images of Fat2-3xGFP's and Lar's localization at the basal surface of an epithelium expressing *Abi-RNAi*. Boxed regions in (A) and (A′) are blown up in the merged image in (B). (B′) Fluorescence intensities and corresponding Pearson's coefficient for Fat2-3xGFP and Lar along the yellow line in (B). Scale bars, 10 μm (A) and 5 μM (B).

(C and D) Rose diagrams showing angular distribution for Fat2-3xGFP and Lar polarity in control (C) and *Abi-RNAi* (D) epithelia. Fat2 and Lar are no longer planar polarized at the basal surface of *Abi-RNAi* epithelia. Six egg chambers were analyzed for each condition. Yellow lines indicate average angle and magnitude of polarity.

Experiments performed at stage 7.

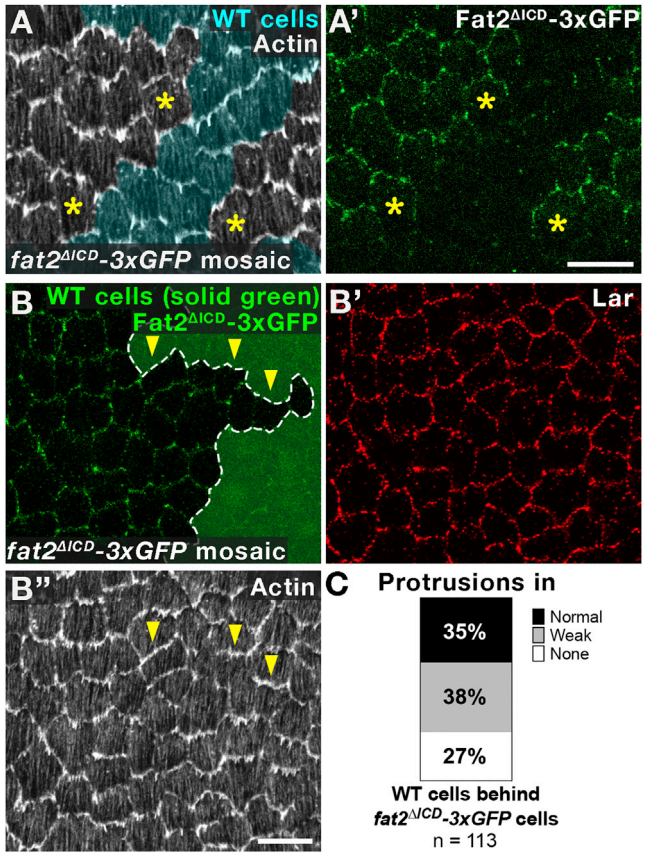

Figure 6. Fat2's Intracellular Domain Is Largely Dispensable for Lar Localization and Protrusion Formation

(A and A′) Image of the basal surface of a *fat2$^{\Delta ICD}$-3xGFP* mosaic epithelium. Wild-type cells are pseudocolored cyan. Fat2$^{\Delta ICD}$-3xGFP protein is localized to the trailing and lateral edges of each cell, but is excluded from the leading edge. Asterisks mark selected cells at the front of the clone. Although we cannot distinguish between homozygous and heterozygous *fat2$^{\Delta ICD}$-3xGFP* cells, we see this localization pattern in all *fat2$^{\Delta ICD}$-3xGFP* mosaics. Scale bar, 10 μm.

(B) Image of the basal surface of *fat2$^{\Delta ICD}$-3xGFP* mosaic epithelium. Wild-type cells express cytoplasmic GFP, and homozygous *fat2$^{\Delta ICD}$-3xGFP* cells lack cytoplasmic GFP. The clone boundary is also indicated by the white dashed line. Fat2$^{\Delta ICD}$-3xGFP stabilizes Lar in the plasma membrane (B′) and non-cell-autonomously induces protrusions in neighboring wild-type cells (triangles) (B″). Scale bar, 10 μm.

(C) Quantification of protrusions in wild-type cells directly behind *fat2$^{\Delta ICD}$-3xGFP* cells.

Experiments performed at stage 7. Images oriented with direction of migration down.

See also Figures S4 and S5.

that tissue movement plays an important role in establishing and/or maintaining Fat2's and Lar's planar polarized localizations.

Fat2's Extracellular Domain Is Sufficient to Stabilize Lar and Induce Protrusions

Our data show that Fat2 acts non-cell-autonomously to affect both protrusion formation and Lar localization at the leading edge of the cell directly behind. Thus, we next investigated whether Fat2's extracellular domain (ECD) mediates these functions. Using the CRISPR-Cas9 system, we generated *fat2$^{\Delta ICD}$-3xGFP*, an allele in which Fat2's intracellular domain (ICD) is replaced with *3xGFP* (Figures S4A–S4C). Fat2$^{\Delta ICD}$-3xGFP has an expanded localization pattern at the basal surface (Figures S4D–S4G), consistent with what has been reported for a similar Fat2 truncation (Aurich and Dahmann, 2016). Mosaic analysis revealed, however, that although Fat2$^{\Delta ICD}$-3xGFP is distributed along both the trailing and lateral edges of each cell's basal surface, it is still excluded from the leading edge (Figure 6A).

To determine whether Fat2's ECD can stabilize Lar in the plasma membrane, we analyzed Lar localization in *fat2$^{\Delta ICD}$-3xGFP* mosaic epithelia. Unlike in *fat2* null clones, where Lar levels are reduced at the basal surface (Figure 4D), Lar levels are normal in *fat2$^{\Delta ICD}$-3xGFP* clones (Figure 6B). Moreover, similar to the truncated Fat2 protein, Lar localization expands to include lateral cell edges, with Fat2$^{\Delta ICD}$-3xGFP and Lar once again showing strong colocalization in puncta (Figures 6B and S4D–S4G). Lar levels are also normal at the basal epithelial surface of homozygous *fat2$^{\Delta ICD}$-3xGFP* egg chambers (Figures S4H–S4J). Hence, Fat2's ECD mediates its role in Lar stabilization and can recruit Lar to ectopic locations.

To determine whether Fat2's ECD can induce protrusions in neighboring cells, we also examined these structures in *fat2$^{\Delta ICD}$-3xGFP* mosaic epithelia. Protrusions are present in a majority of the cells in a *fat2$^{\Delta ICD}$-3xGFP* clone, as well as in the wild-type cells directly behind *fat2$^{\Delta ICD}$-3xGFP* cells (Figures 6B and 6C). Despite its expanded localization pattern, Fat2$^{\Delta ICD}$-3xGFP primarily induces protrusions at the leading edges of neighboring cells, which suggests that there may be a mechanism operating at lateral cell edges to inhibit protrusion formation. Protrusions also form at the basal epithelial surface of homozygous *fat2$^{\Delta ICD}$-3xGFP* egg chambers (Figures S4H–S4J). Altogether, our data suggest that Fat2's ECD extends from each cell's trailing edge to induce protrusions in the cells directly behind, in part by stabilizing Lar at the leading edge of these cells.

Fat2 Stabilizes Lar's Localization at Cell-Cell Interfaces in Dissociated Follicle Cells

As a final test of Fat2's ability to stabilize Lar, we examined these proteins in either single follicle cells or small clusters of follicle cells that had been isolated from follicular epithelia. In single cells, Fat2-3xGFP has a punctate appearance, but Lar is largely undetectable (Figures S5A and S5B). By contrast, small clusters of cells show high levels of both Fat2-3xGFP and Lar co-localizing at cell-cell interfaces (Figure S5C). These data suggest that Lar is unstable at the plasma membrane unless it can interact with another factor on an adjacent cell. We further found that this stabilization of Lar at cell-cell interfaces depends on Fat2 (Figure S5D), and that Fat2's ECD alone is sufficient to stabilize Lar (Figure S5E). By contrast Fat2 continues to localize to cell-cell interfaces in the absence of Lar (Figure S5F). These data show that Fat2 cannot stabilize Lar's plasma membrane localization in *cis*. Instead, Fat2 and Lar must be present on adjacent cells for a *trans* interaction, whether it be direct or indirect, to occur.

Cell-Cell Signaling and Protrusions Both Contribute to Trailing Edge Retraction

Because leading and trailing edge dynamics need to be coordinated between neighboring epithelial cells during their collective migration, we next investigated whether Fat2 and Lar also play a role in trailing edge retraction. We previously showed that when a follicle cell has a defect in this process, its basal surface becomes elongated in the direction of tissue movement (Lewellyn et al., 2013). When the basal surface is elongated in this way, its shape can be variable, with the trailing edge having either a tapered or a more rectangular morphology. This phenotype is difficult to see with an actin label alone, and is best observed either by expressing a fluorescent protein throughout the cell or by staining for a cortical protein such as Discs large (Dlg). Using these methods to label mosaic epithelia, we found that *fat2-RNAi* and *fat2* null cells have elongated basal surfaces (Figures 7A, S6A, and S6B). Moreover, wild-type cells positioned directly ahead of *Lar* null cells also show this distinctive phenotype (Figure 7B). These data suggest that, similar to their function in leading edge protrusion formation, Fat2 and Lar may also work together to control trailing edge retraction.

To investigate how Fat2 and Lar affect this process, we developed a method to quantify trailing edge retraction defects in individual follicle cells (Figure 7C). When the basal surface is elongated, the rest of the cell largely retains its cuboidal shape. Thus, the position of the nucleus is constrained by the cell's lateral membranes, making it a reasonable proxy for the cell's center. We took two measurements at the basal surface of each cell: (1) the distance from the center of the nucleus to the leading edge, and (2) the distance from the center of the nucleus to the trailing edge. In control cells, the nucleus is equidistant from both leading and trailing edges (Figures 7D, S6A, and S6E). In elongated cells, however, the distance between the nucleus and the trailing edge increases, while the nucleus' distance to the leading edge remains the same (Figures 7D and S6E).

We hypothesized that Fat2 and Lar might influence trailing edge retraction through a protrusion-based mechanism, wherein Fat2 and Lar induce leading edge protrusions, and the protrusions help to release the trailing edge of the cell ahead, perhaps via mechanical means. To test this idea, we generated clones of *SCAR* (also known as Wave) mutant cells, which lack leading edge protrusions on a cell-autonomous basis (Cetera et al., 2014). Wild-type cells positioned directly ahead of *SCAR* cells show a moderate extension of their trailing edges (Figures 7D and S6C). However, this phenotype is weaker than that seen in wild-type cells positioned directly ahead of *Lar* null cells (Figure 7D), even though *Lar* cells retain some protrusive activity (Figure 3G). Indeed, we have observed wild-type cells with extended trailing edges directly ahead of *Lar* cells where obvious protrusions are present (Figure S6F). Thus, our data suggest that leading edge protrusions likely do contribute to trailing edge retraction in the cell ahead, but that Lar also plays a signaling role in this process that is independent of its role in protrusion formation.

We next explored whether Fat2 might transduce the retraction signal from Lar. If so, this process should require Fat2's ICD. Within a mosaic epithelium, *fat2$^{\Delta ICD}$-3xGFP* cells show a moderate extension of their trailing edges; however, this extension is less than that seen in *fat2* null cells (Figures 7D and S6D). This observation makes sense, because *fat2$^{\Delta ICD}$-3xGFP* cells can still induce protrusions in the cell behind and *fat2* null cells cannot. Altogether, our data suggest that Lar signals from the leading edge to promote retraction in the cell ahead, and that Fat2 plays a cell-autonomous role in this process; however, more work will be required to determine whether Lar signals via Fat2.

Although we have attempted to identify the mechanism by which Fat2 promotes trailing edge retraction on a cell-autonomous basis, we have thus far only obtained three negative results. First, we asked whether Fat2 signals through Misshapen (Msn) kinase, as Msn is enriched at follicle cell trailing edges,

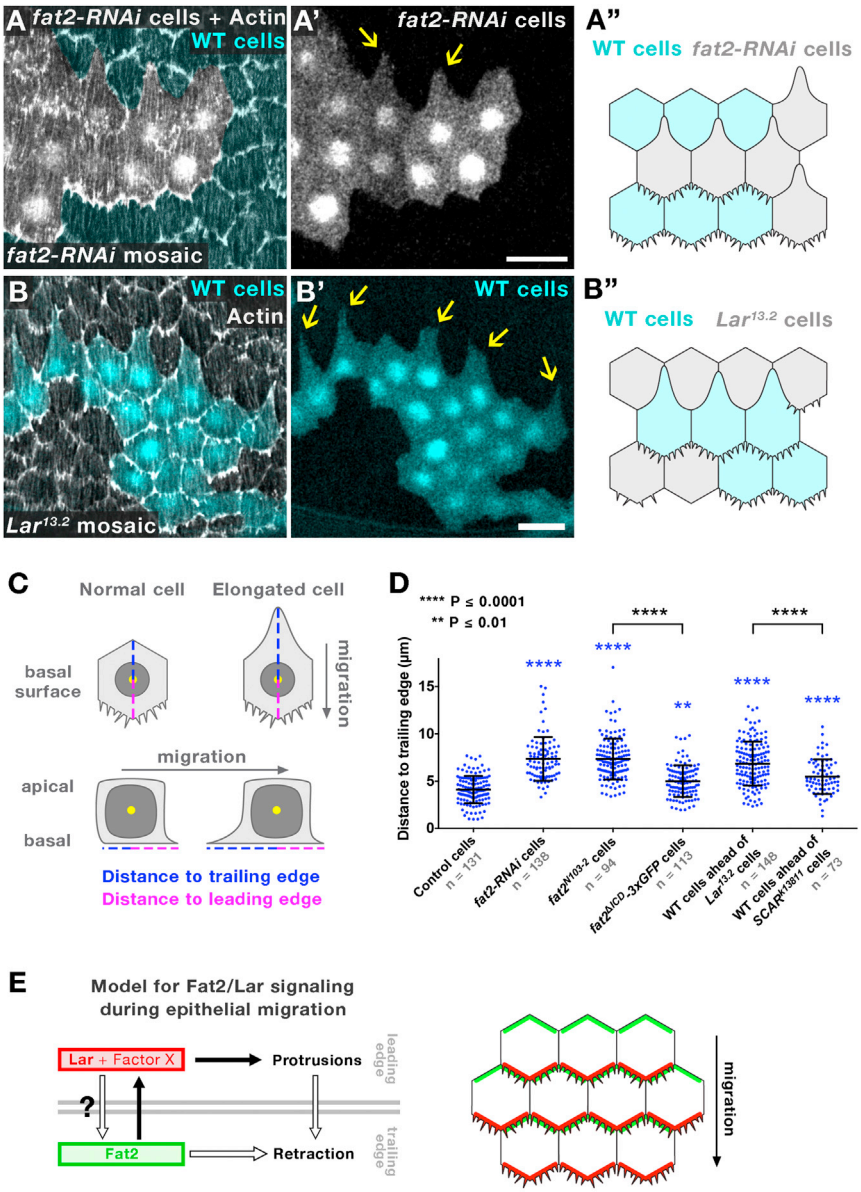

Figure 7. Cell-Cell Signaling and Protrusions Both Contribute to Trailing Edge Retraction

(A and A′) Fat2 functions cell-autonomously in trailing edge retraction, as *fat2-RNAi* cells have elongated basal surfaces (arrows). The image in (A) is a three-part overlay of actin, fluorescent clone marker, and a cyan pseudocolored mask. Scale bar, 10 μm.

(B and B′) Lar promotes trailing edge retraction non-cell-autonomously. Wild-type cells (cyan) directly ahead of $Lar^{13.2}$ cells have elongated basal surfaces (arrows). Scale bar, 10 μm. Illustrations in (A″) and (B″) depict results shown in micrographs.

(C and D) Quantification of trailing edge retraction defects. The method used to generate data in (D) is depicted in (C). The yellow dot marks the center of the nucleus. (D) In elongated cells, the nuclear distance to the trailing edge increases compared with controls (blue asterisks). In $Lar^{13.2}$ and $SCAR^{k13811}$ mosaics, measurements were made on wild-type cells directly ahead of mutant cells. Individual data points, mean ± SD; one-way ANOVA.

(E) Model for Fat2/Lar signaling during epithelial migration. Arrows indicate the direction of information flow for protrusion formation (black arrows) and trailing edge retraction (white arrows).

Experiments performed at stage 7. Images oriented with direction of migration down.

See also Figures S6 and S7.

and is required cell-autonomously for trailing edge retraction (Lewellyn et al., 2013). We found that Msn localizes normally in *fat2* null cells (Figures S7A and S7B). Moreover, Msn appears to be active in these cells, as small *fat2* clones are carried along the migration path by their wild-type neighbors (Viktorinová and Dahmann, 2013); by contrast, small *msn* clones remain stuck to the ECM due to increased integrin-based adhesion (Lewellyn et al., 2013).

Second, we investigated whether Fat2 works through the microtubule-binding protein CLASP. CLASP targets microtubule plus ends to focal adhesions to promote their disassembly in some cell types (Lim et al., 2016; Stehbens et al., 2014), and *CLASP* genetically interacts with *fat2* (Chen et al., 2016). We found, however, that follicle cells expressing *CLASP-RNAi* do not show defects in trailing edge retraction (Figures S7C and S7D). The RNAi appears to be depleting the CLASP protein, as microtubules are highly reduced in *CLASP-RNAi* cells. However, it is still possible that this is a partial knockdown that is insufficient to elicit a trailing edge phenotype.

Third, we explored whether Fat2 promotes acto-myosin contractility to pull the cell's trailing edge forward, a process that is likely mediated by contractile stress fibers at the basal surface of each cell. We found that myosin levels are normal on the stress fibers in *fat2* null cells (Figures S7E–S7G). These data suggest that active myosin is recruited to the stress fibers normally in the absence of Fat2; however, myosin dynamics could still be affected. Thus, future work will be required to determine how Fat2 and Lar promote trailing edge retraction.

DISCUSSION

Epithelial migration plays essential roles in embryogenesis, wound repair, and the spread of some cancers, yet little is known about how individual cell migratory behaviors are coordinated within an epithelial sheet. In particular, epithelial cells need to coordinate the formation of protrusions at the leading edge of one cell with the retraction of the trailing edge of the cell directly ahead. Through mosaic analyses of a migratory epithelium in *Drosophila*, we have discovered that Fat2 and Lar function in a planar signaling system that coordinates these leading and

trailing edge dynamics between neighboring cells. This finding has important implications for our understanding of collective cell migration, planar cell-cell signaling, and egg chamber elongation, each of which is discussed below.

Fat2 and Lar Coordinate Leading and Trailing Edge Dynamics between Neighboring Cells

Our findings represent a significant shift in our understanding of how Fat2 and Lar promote epithelial motility. A previous model posited that Fat2 and Lar both stimulate the formation of leading edge protrusions in the follicle cells by recruiting actin assembly factors to their ICDs on a cell-autonomous basis (Squarr et al., 2016). Our data show, however, that Fat2 plays a non-cell-autonomous role in protrusion formation and that its ICD is largely dispensable for this process. We propose an alternate mechanism wherein Fat2's ECD extends from each cell's trailing edge to stabilize Lar in the leading plasma membrane of the cell directly behind. This interaction then allows Lar to recruit actin assembly factors to this location. Because the protrusion and motility defects in *Lar* null cells are weaker than those produced by loss of Fat2 (Figures 2D, 3B, and 3G), we further propose that there may be another leading edge transmembrane protein (Factor X) that functions partially redundantly with Lar (Figure 7E). Future work will be required to identify this factor.

This work also introduces a new function for Fat2 and Lar in the control of trailing edge retraction. Specifically, our data suggest that Lar signals from each cell's leading edge to stimulate trailing edge retraction in the cell directly ahead, and that Fat2's ICD may help to transduce this signal. Our data further suggest that leading edge protrusions also aid in the release of the trailing edge of the cell ahead. Thus, Fat2 and Lar likely also affect trailing edge retraction indirectly via their role in protrusion formation. Determining how Fat2/Lar signaling and leading edge protrusions work together to stimulate trailing edge retraction will be an important area for future research.

Altogether, these observations suggest a model wherein Fat2 and Lar promote epithelial motility by coordinating leading and trailing edge dynamics between neighboring cells. Given that Fat2's mammalian homologs have been implicated in both epithelial and non-epithelial collective migrations (Hou and Sibinga, 2009; Moeller et al., 2004; Nishikawa et al., 2011; Tanoue and Takeichi, 2004), this role for Fat2 and Lar may be conserved. Moreover, in *C. elegans*, Fat2 (CDH-4) and Lar (PTP-3) work together to promote Q neuroblast migration, with PTP-3 functioning cell-autonomously in the neuroblast and CDH-4 functioning non-cell-autonomously in an unknown tissue (Sundararajan and Lundquist, 2012; Sundararajan et al., 2014). This observation suggests that Fat2/Lar signaling may also control individual cell motility, although in this case the signaling mechanism would be slightly different. Thus, Fat2/Lar signaling may be a widely used strategy through which cells influence the migratory behavior of their neighbors.

Fat2 and Lar Define a New Planar Signaling System that Promotes Epithelial Motility

It has previously been speculated that Fat2 and/or Lar might mediate planar cell-cell signaling in a manner that is similar to the Fz/Vang and Ft/Ds signaling complexes (Bateman et al., 2001; Frydman and Spradling, 2001; Viktorinova et al., 2009). Our data now show that Fat2/Lar signaling does in fact share certain commonalities with these classic PCP systems. Specifically, Fat2 and Lar localize to opposite sides of each cell and mediate information flow across cell-cell boundaries. They also form distinct, overlapping puncta along cell-cell interfaces, similar to PCP signaling complexes. There are also important differences, however. Whereas the PCP systems operate near the apical surface to transmit long-range positional information across the tissue, the Fat2/Lar system operates near the basal surface to transmit short-range information between adjacent cells. Thus, this work establishes a new paradigm for planar cell-cell signaling.

Our observations that Fat2 and Lar colocalize in puncta, and that they continue to do so under several experimental conditions, suggest that these proteins function in discrete signaling centers that span cell-cell boundaries. Our data further show that these centers signal with high spatial resolution, as we can detect phenotypes from loss of signaling on the sub-cellular level (Figures 3D–3F). It is important to note, however, that although Fat2 recruits Lar into the puncta via its ECD, there is currently no evidence that Fat2 and Lar bind to one another directly. It is equally possible that the Fat2-Lar interaction is bridged by one or more transmembrane proteins that remain to be identified, such as the hypothetical Factor X.

Although Fat2 stabilizes Lar's localization at the leading edge of the cell behind, Lar plays a far less important role in localizing Fat2. Previous studies have proposed that Fat2 attains its trailing edge localization via a feedback amplification loop involving microtubules (Aurich and Dahmann, 2016; Viktorinová and Dahmann, 2013). In support of this idea, Fat2 is required for the bias in the direction of microtubule plus-end growth before epithelial migration begins, an event that may determine the direction of migration (Chen et al., 2016). We have been unable to detect planar polarization of Fat2-3xGFP during this period, suggesting that Fat2 both contributes and responds to this symmetry-breaking event. We have also discovered that tissue migration is required for Fat2's trailing edge localization (Figure 5). Whether this effect occurs because migration helps to organize microtubules or whether migration represents a separate input into the Fat2 localization mechanism is currently unknown.

Fat2 and Lar Likely Promote Egg Chamber Elongation via Their Roles in Epithelial Migration

Finally, this work helps to clarify how Fat2's and Lar's roles in epithelial motility relate to their roles in egg chamber elongation (Bateman et al., 2001; Frydman and Spradling, 2001; Viktorinova et al., 2009). Although initially spherical, egg chambers lengthen as they mature. This process occurs, in part, although a "molecular corset" mechanism, wherein parallel arrays of stress fibers at the basal surface of each follicle cell become aligned orthogonal to the elongation axis. The resulting circumferential organization of these structures is then thought to help anisotropically channel egg chamber growth, thus creating the elongated shape of the egg.

Fat2 and Lar have been shown to have non-autonomous effects on the tissue-level alignment of the stress fibers in the molecular corset (Bateman et al., 2001; Frydman and Spradling, 2001; Viktorinova et al., 2009). However, Fat2's and Lar's roles

in this process ultimately depend on the short-range non-cell-autonomous roles we have identified for Fat2 and Lar in protrusion formation and trailing edge retraction, respectively. Tissue-level stress fiber alignment is an all-or-nothing process that depends on the percentage of non-migratory cells within the epithelium. For example, when *fat2* cells make up less than 60% of the epithelium, the stress fibers are globally aligned; when *fat2* cells exceed 60%, stress fiber alignment is globally perturbed (Viktorinova et al., 2009). This observation and others have led to the model that the deciding factor between global stress fiber alignment and global perturbation is whether there are enough wild-type cells in the epithelium for tissue migration to proceed (for a more thorough discussion of this topic, see Cetera and Horne-Badovinac, 2015). In contrast, the non-cell-autonomous defects we have identified in *fat2* and *Lar* mosaic epithelia are independent of clone size, and only extend one cell diameter away from the clone. Thus, Fat2's and Lar's true non-autonomous functions are to promote epithelial motility, and epithelial motility, in turn, aligns the stress fibers.

The idea that epithelial motility globally aligns the stress fibers was challenged by a recent study, however (Aurich and Dahmann, 2016). This study used a fosmid construct, wherein Fat2's ICD was removed (Fat2$^{\Delta ICR}$), to rescue a *fat2* allele. They reported that Fat2$^{\Delta ICR}$ is not planar polarized. They also reported that, although this genetic condition appeared to block epithelial migration, tissue-level stress fiber alignment and egg chamber elongation were both largely normal. Fat2$^{\Delta ICR}$ is similar to the Fat2$^{\Delta ICD}$-3xGFP generated in our study; however, there are three key differences. First, Fat2$^{\Delta ICD}$-3xGFP was made using the CRISPR/Cas9 system to directly edit the *fat2* locus. Second, Fat2$^{\Delta ICD}$-3xGFP shows an expanded localization, but it is still absent from each cell's leading edge. The previously published Fat2$^{\Delta ICR}$ construct may in fact show this same localization, but mosaic analyses would be required to confirm this. Third, roughly two-thirds of the eggs produced by homozygous *fat2$^{\Delta ICD}$-3xGFP* females are round (Figure S4C). Thus, elongation is normal in a subset of *fat2$^{\Delta ICD}$-3xGFP* egg chambers, but not in all of them.

One important outcome from the present study is a possible explanation for why tissue-level stress fiber alignment can still occur in the absence of epithelial movement. We have shown that Fat2's ECD is sufficient to induce leading edge protrusions in the cell directly behind. We propose, therefore, that leading edge protrusive activity may provide a transmittable polarizing cue that is sufficient to globally align stress fibers, perhaps via mechanical means. We further propose that the reason epithelial migration fails in the Fat2$^{\Delta ICR}$ condition is due to the need for Fat2's ICD in trailing edge retraction (this study) and/or microtubule organization (Aurich and Dahmann, 2016). In this model, individual cell migratory behaviors would still be the driving force behind global stress fiber alignment even in the absence of epithelial movement, consistent with the large number of studies that have implicated the migration machinery in this process (Bateman et al., 2001; Cetera et al., 2014; Chen et al., 2016; Haigo and Bilder, 2011; Lewellyn et al., 2013; Squarr et al., 2016).

Altogether, our work on Fat2 and Lar defines a key mechanism promoting epithelial migration, establishes a new paradigm for planar cell-cell signaling, and helps to elucidate how epithelial migration can influence tissue morphogenesis.

STAR★METHODS

Detailed methods are provided in the online version of this paper and include the following:

- KEY RESOURCES TABLE
- CONTACT FOR REAGENT AND RESOURCE SHARING
- EXPERIMENTAL MODEL AND SUBJECT DETAILS
- METHOD DETAILS
  - *Drosophila* Genetics
  - Clone Labeling Method
  - Time-Lapse Image Acquisition and Microscopy
  - Fixed Image Acquisition and Microscopy
  - Follicle Cell Primary Cultures
  - Quantification of Protrusions
  - Quantification of Fat2 and Lar Colocalization
  - Quantification of Fat2 and Lar Polarity
  - Nuclear Positioning Measurements
  - Generation of Fat2-3xGFP and Fat2$^{\Delta ICD}$-3xGFP
  - Quantification of Egg Aspect Ratio
  - Quantification of Sqh-GFP Fluorescence
- QUANTIFICATION AND STATISTICAL ANALYSIS

SUPPLEMENTAL INFORMATION

Supplemental Information includes seven figures, two tables, one data file, and one movie and can be found with this article online at http://dx.doi.org/10.1016/j.devcel.2017.02.003.

AUTHOR CONTRIBUTIONS

K.B., M.C., and S.H.-B. designed the experiments. K.B. and M.C. performed the experiments and analyzed the data. K.B. generated new reagents and prepared the figures. K.B. and S.H.-B. wrote the manuscript.

ACKNOWLEDGMENTS

We thank the flyCRISPR group at UW-Madison for advice, Yi Guo, Jennifer Zallen, and Allan Spradling for *Drosophila* stocks, Ben Glick for 3xGFP plasmid, Darcy Andersen and Kayla Muirhead for experimental assistance, and Nick Badovinac and Nate Ellis for illustrations. We thank Benoit Aiguoy for providing Packing Analyzer, and Wen Yih Aw, Bryan Heck, and Danelle Devenport for providing the MATLAB script to normalize and plot polarity data. Ellie Heckscher, Chip Ferguson, Ed Munro, Volodya Gelfand, and members of the Horne-Badovinac lab provided valuable comments on the manuscript. K.B. is an HHMI Fellow of the Life Sciences Research Foundation. This work was further supported by NIH grants T32 GM007183 (to M.C.) and R01 GM094276 (to S.H.-B.).

Received: August 10, 2016
Revised: December 20, 2016
Accepted: February 6, 2017
Published: March 13, 2017

REFERENCES

Aigouy, B., Farhadifar, R., Staple, D.B., Sagner, A., Röper, J.-C., Jülicher, F., and Eaton, S. (2010). Cell flow reorients the axis of planar polarity in the wing epithelium of *Drosophila*. Cell *142*, 773–786.

Aurich, F., and Dahmann, C. (2016). A mutation in fat2 uncouples tissue elongation from global tissue rotation. Cell Rep. *14*, 2503–2510.

Aw, W.Y., Heck, B.W., Joyce, B., and Devenport, D. (2016). Transient tissue-scale deformation coordinates alignment of planar cell polarity junctions in the mammalian skin. Curr. Biol. *26*, 2090–2100.

Bateman, J., Reddy, R.S., Saito, H., and Van Vactor, D. (2001). The receptor tyrosine phosphatase Dlar and integrins organize actin filaments in the *Drosophila* follicular epithelium. Curr. Biol. *11*, 1317–1327.

Cetera, M., and Horne-Badovinac, S. (2015). Round and round gets you somewhere: collective cell migration and planar polarity in elongating *Drosophila* egg chambers. Curr. Opin. Genet. Dev. *32*, 10–15.

Cetera, M., Ramirez-San Juan, G.R., Oakes, P.W., Lewellyn, L., Fairchild, M.J., Tanentzapf, G., Gardel, M.L., and Horne-Badovinac, S. (2014). Epithelial rotation promotes the global alignment of contractile actin bundles during *Drosophila* egg chamber elongation. Nat. Commun. *5*, 5511.

Cetera, M., Lewellyn, L., and Horne-Badovinac, S. (2016). Cultivation and live imaging of *Drosophila* ovaries. In *Drosophila* Oogenesis, Methods in Molecular Biology, D.P. Bratu and G.P. McNeil, eds. (Springer New York), pp. 215–226.

Chen, D.-Y., Lipari, K.R., Dehghan, Y., Streichan, S.J., and Bilder, D. (2016). Symmetry breaking in an edgeless epithelium by Fat2-regulated microtubule polarity. Cell Rep. *15*, 1125–1133.

Devenport, D. (2014). Cell biology in development: the cell biology of planar cell polarity. J. Cell Biol. *207*, 171–179.

Friedl, P., and Gilmour, D. (2009). Collective cell migration in morphogenesis, regeneration and cancer. Nat. Rev. Mol. Cell Biol. *10*, 445–457.

Frydman, H.M., and Spradling, A.C. (2001). The receptor-like tyrosine phosphatase lar is required for epithelial planar polarity and for axis determination within *Drosophila* ovarian follicles. Development *128*, 3209–3220.

Gratz, S.J., Cummings, A.M., Nguyen, J.N., Hamm, D.C., Donohue, L.K., Harrison, M.M., Wildonger, J., and O'Connor-Giles, K.M. (2013). Genome engineering of *Drosophila* with the CRISPR RNA-guided Cas9 nuclease. Genetics *194*, 1029–1035.

Gratz, S.J., Ukken, F.P., Rubinstein, C.D., Thiede, G., Donohue, L.K., Cummings, A.M., and O'Connor-Giles, K.M. (2014). Highly specific and efficient CRISPR/Cas9-Catalyzed homology-directed repair in *Drosophila*. Genetics *196*, 961–971.

Gutzeit, H.O., Eberhardt, W., and Gratwohl, E. (1991). Laminin and basement membrane-associated microfilaments in wild-type and mutant *Drosophila* ovarian follicles. J. Cell Sci. *100*, 781–788.

Haigo, S.L., and Bilder, D. (2011). Global tissue revolutions in a morphogenetic movement controlling elongation. Science *331*, 1071–1074.

Hale, R., Brittle, A.L., Fisher, K.H., Monk, N.A.M., and Strutt, D. (2015). Cellular interpretation of the long-range gradient of Four-jointed activity in the *Drosophila* wing. Elife *4*.

Horne-Badovinac, S., Hill, J., Gerlach, G., Menegas, W., and Bilder, D. (2012). A screen for round egg mutants in *Drosophila* identifies tricornered, furry, and misshapen as regulators of egg chamber elongation. G3 (Bethesda) *2*, 371–378.

Hou, R., and Sibinga, N.E.S. (2009). Atrophin proteins interact with the Fat1 cadherin and regulate migration and orientation in vascular smooth muscle cells. J. Biol. Chem. *284*, 6955–6965.

Isabella, A.J., and Horne-Badovinac, S. (2016). Rab10-Mediated secretion synergizes with tissue movement to build a polarized basement membrane architecture for organ morphogenesis. Dev. Cell *38*, 47–60.

Lewellyn, L., Cetera, M., and Horne-Badovinac, S. (2013). Misshapen decreases integrin levels to promote epithelial motility and planar polarity in *Drosophila*. J. Cell Biol. *200*, 721–729.

Lim, B.C., Matsumoto, S., Yamamoto, H., Mizuno, H., Kikuta, J., Ishii, M., and Kikuchi, A. (2016). Prickle1 promotes focal adhesion disassembly in cooperation with the CLASP-LL5β complex in migrating cells. J. Cell Sci. *129*, 3115–3129.

Lye, C.M., Naylor, H.W., and Sanson, B. (2014). Subcellular localisations of the CPTI collection of YFP-tagged proteins in *Drosophila* embryos. Development *141*, 4006–4017.

Matis, M., and Axelrod, J.D. (2013). Regulation of PCP by the Fat signaling pathway. Genes Dev. *27*, 2207–2220.

Mayor, R., and Etienne-Manneville, S. (2016). The front and rear of collective cell migration. Nat. Rev. Mol. Cell Biol. *17*, 97–109.

Moeller, M.J., Soofi, A., Braun, G.S., Li, X., Watzl, C., Kriz, W., and Holzman, L.B. (2004). Protocadherin FAT1 binds Ena/VASP proteins and is necessary for actin dynamics and cell polarization. EMBO J. *23*, 3769–3779.

Nishikawa, Y., Miyazaki, T., Nakashiro, K.-I., Yamagata, H., Isokane, M., Goda, H., Tanaka, H., Oka, R., and Hamakawa, H. (2011). Human FAT1 cadherin controls cell migration and invasion of oral squamous cell carcinoma through the localization of β-catenin. Oncol. Rep. *26*, 587–592.

Pocha, S.M., and Montell, D.J. (2014). Cellular and molecular mechanisms of single and collective cell migrations in *Drosophila*: themes and variations. Annu. Rev. Genet. *48*, 295–318.

Prasad, M., Jang, A.C.-C., Starz-Gaiano, M., Melani, M., and Montell, D.J. (2007). A protocol for culturing *Drosophila* melanogaster stage 9 egg chambers for live imaging. Nat. Protoc. *2*, 2467–2473.

Sarov, M., Barz, C., Jambor, H., Hein, M.Y., Schmied, C., Suchold, D., Stender, B., Janosch, S., K J, V.V., Krishnan, R.T., et al. (2016). A genome-wide resource for the analysis of protein localisation in *Drosophila*. Elife *5*, e12068.

Sebo, Z.L., Lee, H.B., Peng, Y., and Guo, Y. (2014). A simplified and efficient germline-specific CRISPR/Cas9 system for Drosophila genomic engineering. Fly (Austin) *8*, 52–57.

Squarr, A.J., Brinkmann, K., Chen, B., Steinbacher, T., Ebnet, K., Rosen, M.K., and Bogdan, S. (2016). Fat2 acts through the WAVE regulatory complex to drive collective cell migration during tissue rotation. J. Cell Biol. *212*, 591–603.

Stehbens, S.J., Paszek, M., Pemble, H., Ettinger, A., Gierke, S., and Wittmann, T. (2014). CLASPs link focal-adhesion-associated microtubule capture to localized exocytosis and adhesion site turnover. Nat. Cell Biol. *16*, 561–573.

Strutt, H., Warrington, S.J., and Strutt, D. (2011). Dynamics of core planar polarity protein turnover and stable assembly into discrete membrane subdomains. Dev. Cell *20*, 511–525.

Sundararajan, L., and Lundquist, E.A. (2012). Transmembrane proteins UNC-40/DCC, PTP-3/LAR, and MIG-21 control anterior-posterior neuroblast migration with left-right functional asymmetry in Caenorhabditis elegans. Genetics *192*, 1373–1388.

Sundararajan, L., Norris, M.L., Schöneich, S., Ackley, B.D., and Lundquist, E.A. (2014). Developmental biology. Dev. Biol. *392*, 141–152.

Tanoue, T., and Takeichi, M. (2004). Mammalian Fat1 cadherin regulates actin dynamics and cell-cell contact. J. Cell Biol. *165*, 517–528.

Viktorinová, I., and Dahmann, C. (2013). Microtubule polarity predicts direction of egg chamber rotation in *Drosophila*. Curr. Biol. *23*, 1472–1477.

Viktorinova, I., Konig, T., Schlichting, K., and Dahmann, C. (2009). The cadherin Fat2 is required for planar cell polarity in the *Drosophila* ovary. Development *136*, 4123–4132.

Zallen, J.A., Cohen, Y., Hudson, A.M., Cooley, L., Wieschaus, E., and Schejter, E.D. (2002). SCAR is a primary regulator of Arp2/3-dependent morphological events in *Drosophila*. J. Cell Biol. *156*, 689–701.

STAR★METHODS

KEY RESOURCES TABLE

REAGENT or RESOURCE	SOURCE	IDENTIFIER
Antibodies		
Mouse monoclonal anti-Lar	Developmental Studies Hybridoma Bank	9D82B3; RRID: AB_528202
Rat monoclonal anti-NCad	Developmental Studies Hybridoma Bank	DN-ex #8
Mouse monoclonal anti-Dlg	Developmental Studies Hybridoma Bank	4F3; RRID: AB_528203
Mouse monoclonal anti-acetylated-α-tubulin	Santa Cruz Biotechnology	Clone 6-11B-1; RRID: AB_628409
Rabbit polyclonal anti-GFP directly coupled to Alexa Fluor-488	Invitrogen	A21311
AlexaFluor-488 donkey anti-mouse secondary	ThermoFisher	A21202; RRID: AB_2535788
AlexaFluor-555 donkey anti-mouse secondary	ThermoFisher	A31570; RRID: AB_2536180
AlexaFluor-488 goat anti-rat secondary	ThermoFisher	A11006; RRID: AB_2534074
AlexaFluor-555 goat anti-rat secondary	ThermoFisher	A11081
Chemicals, Peptides, and Recombinant Proteins		
Recombinant human insulin	Sigma	12643
CellMask Deep Red Plasma Membrane Stain	ThermoFisher	C1006
collagenase	Sigma	C6885
Schneider's Drosophila medium	ThermoFisher	21720-024
NuSieve GTG low-melt agarose	Lonza	50081
Gas permeable membrane slides	Sarstedt x-well	94.6150.101
Halocarbon oil 27	Sigma	H8773
16% EM grade formaldehyde	Polysciences Inc	18814-10
Phalloidin-TRITC	Sigma	P1951
AlexaFluor-647 phalloidin	ThermoFisher	A22287
DAPI	Sigma	D9542
Alfa Aesar Concanavalin A	Fisher	11028-71-0
Slowfade antifade kit	ThermoFisher	S2828
Fisherbrand cover glass 22 mm x 50 mm	Fisher	12-544-D
Fisherbrand cover glass 22 mm x 30 mm	Fisher	12-544-A
Fisherbrand cover glass 22 mm x 22 mm	Fisher	12-542-B
Experimental Models: Organisms/Strains		
D. melanogaster. Standard control strain: w[1118]	Bloomington Drosophila Stock Center	BDSC: 3605; FlyBase ID: FBst0003605
D. melanogaster. fat2-3xGFP, FRT80B	This paper	N/A
D. melanogaster. fat2ΔICD-3xGFP, FRT80B	This paper	N/A
D. melanogaster. Lar[bola1]	Laboratory of Allan Spradling; Frydman and Spradling, 2001.	FlyBase ID: FBal0095667
D. melanogaster. Lar[bola2]	Laboratory of Allan Spradling; Frydman and Spradling, 2001.	Flybase ID: FBal0095666
D. melanogaster. w*; Lar13.2, FRT40A	Laboratory of David Van Vactor; Bateman et al., 2001.	Flybase ID: FBst0008774
D. melanogaster. fat2[N103-2], FRT80B	Laboratory of Sally Horne-Badovinac; Horne-Badovinac et al., 2012	FlyBase ID: FBal0267777
D. melanogaster. fat2[G58-2], FRT80B	Laboratory of Sally Horne-Badovinac; Horne-Badovinac et al., 2012	FlyBaseID: FBal0267775
D. melanogaster. P[lacW]SCAR[k13811], FRT40A	Laboratory of Jennifer Zallen; Zallen et al., 2002	FlyBase ID: FBal0150644
D. melanogaster. RNAi of Abi:	National Institute of Genetics, Japan	NIG: 9749R-3

(*Continued on next page*)

Continued

REAGENT or RESOURCE	SOURCE	IDENTIFIER
D. melanogaster. RNAi of Fat2: y[1] v[1]; P{y[+t7.7] v[+t1.8]=TRiP.HMS02136}attP40	Bloomington Drosophila Stock Center	BDSC: 40888; FlyBase ID: FBst0040888
D. melanogaster. RNAi of CLASP: y[1] sc[*] v[1]; P{y[+t7.7] v[+t1.8]=TRiP.GL00367}attP2	Bloomington Drosophila Stock Center	BDSC: 35442; FlyBase ID: FBst0035442
D. melanogaster. Msn-YFP: w1118; PBac{802.P.SVS-2}msnCPTI003908	Kyoto Stock Center	DGRC: 115454
D. melanogaster. Sqh-GFP: Sqh-2xTY1-SGFP-3xFLAG	Vienna Drosophila Resource Center	VDRC: 318484
D. melanogaster. y[1] w[*]; P{w[+mW.hs]=en2.4-GAL4}e22c P{w[+mC]=UAS-FLP.D}JD1/CyO	Bloomington Drosophila Stock Center	BDSC: 5083; FlyBaseID: FBst0005083
D. melanogaster. P{ry[+t7.2]=neoFRT}40A/CyO; P{w[+mW.hs]=GawB}T155 P{w[+mC]=UAS-FLP.D}JD2/TM3, Sb[1]	Bloomington Drosophila Stock Center	BDSC: 5074; FlyBase ID: FBst0005074
D. melanogaster. w[1118]; P{w[+mC]=Ubi-GFP(S65T)nls}2L P{ry[+t7.2]=neoFRT}40A/CyO	Bloomington Drosophila Stock Center	BDSC: 5629; FlyBase ID: FBst0005629
D. melanogaster. y[1] w[1118]; P{w[+mC]=Ubi-mRFP.nls}2L P{ry[+t7.2]=neoFRT}40A/CyO	Bloomington Drosophila Stock Center	BDSC: 34500; FlyBase ID: FBst0034500
D. melanogaster. w[1118]; P{w[+mC]=Ubi-mRFP.nls}3L P{ry[+t7.2]=neoFRT}80B	Bloomington Drosophila Stock Center	BDSC: 30852; FlyBase ID: FBst0030852
D. melanogaster. w[*]; P{w[+mC]=Ubi-GFP.D}61EF P{ry[+t7.2]=neoFRT}80B	Bloomington Drosophila Stock Center	BDSC: 1620; FlyBase ID FBst0001620
D. melanogaster. traffic jam-Gal4: y* w*; P{w+mW.hs=GawB}NP1624 / CyO, P{w-=UAS-lacZ.UW14}UW14	Kyoto Stock Center	DGRC: 104055
D. melanogaster. w[1118]; P{w[+mC]=GAL4-Act5C(FRT.CD2).P}S, P{w[+mC]=UAS-RFP.W}3/TM3, Sb[1]	Bloomington Drosophila Stock Center	BDSC: 30558; FlyBase ID: FBst0030558
D. melanogaster. P{ry[+t7.2]=hsFLP}22, w[*]	Bloomington Drosophila Stock Center	BDSC: 8862; FlyBase ID: FBst0008862
D. melanogaster. y[1] M{vas-Cas9.S}ZH-2A w[1118] [RFP-mutated]	Laboratory of Yi Guo, Sebo et al., 2014	N/A
D. melanogaster. Cre-expressing: y[1] w[67c23]; MKRS, P{ry[+t7.2]=hsFLP}86E/TM6B, P{w[+mC]=Crew}DH2, Tb[1]	Bloomington Drosophila Stock Center	BDSC: 1501; Flybase ID:
Oligonucleotides		
Primer for fat2 gRNA (forward): CTTCGGAGGGGCCGATTTCTAGGA	This paper	N/A
Primer for fat2 gRNA (reverse): AAACTCCTAGAAATCGGCCCCTCC	This paper	N/A
Primer for fat2$^{\Delta ICD}$ gRNA (forward): CTTCGAACAAGTCGTCGTACAAGG	This paper	N/A
Primer for fat2$^{\Delta ICD}$ gRNA (reverse): AAACCCTTGTACGACGACTTGTTC	This paper	N/A
Recombinant DNA		
Plasmid: fat2-3xGFP floxDsRed, see Data S1	This paper	N/A
Plasmid: fat2$^{\Delta ICD}$-3xGFP floxDsRed, see Data S1	This paper	N/A
Plasmid: pU6:2 fat2 chiRNA v2	This paper	N/A
Plasmid: pU6:2 proximal-ICD chiRNA	This paper	N/A
Plasmid: pU6-BbsI-chiRNA	Gratz et al., 2013	N/A
Plasmid – 3xP3-RFP source: pHD-DsRed-attP	Gratz et al., 2014	N/A
Plasmid – 3xGFP source: pmEGFP-13	Addgene	36410
Plasmid: pUC19	ThermoFisher	SD0061
Software and Algorithms		
Packing Analyzer V2	Aigouy et al., 2010	https://grr.gred-clermont.fr/labmirouse/software/WebPA/index.html

(*Continued on next page*)

Continued

REAGENT or RESOURCE	SOURCE	IDENTIFIER
ImageJ Version 2.0.0-rc-43/1.51h		https://fiji.sc/
KymoResliceWide Plugin version 0.4		http://imagej.net/KymoResliceWide
Matlab Version R2015a (8.5.0)	Mathworks	N/A
Prism Version 6	Graphpad	N/A

CONTACT FOR REAGENT AND RESOURCE SHARING

Further information and requests for resources and reagents should be directed to and will be fulfilled by the Lead Contact, Sally Horne-Badovinac (shorne@uchicago.edu).

EXPERIMENTAL MODEL AND SUBJECT DETAILS

D. melanogaster was cultured on cornmeal molasses agar food using standard techniques. All experiments were performed on adult females. Experimental crosses were raised at 25C. Experimental females (1-3 days old) were aged on yeast with males for 1-2 days at 25C.

METHOD DETAILS

Drosophila Genetics

Detailed information about source strains is listed in the Key Resources table. Detailed experimental genotypes are listed in Table S2. All mutant alleles used in this study are nulls except $SCAR^{k13811}$, which is a strong hypomorph (Zallen et al., 2002). Stocks are from the Bloomington *Drosophila* Stock Center with the following exceptions. Lar^{bola1} and Lar^{bola2} are from Frydman and Spradling (2001). $SCAR^{k13811}$ is from Zallen et al. (2002). $fat2^{N103-2}$ and $fat2^{G58-2}$ are from Horne-Badovinac et al. (2012). $Lar^{13.2}$, *FRT40* is from Bateman et al. (2001). *Traffic jam-Gal4* (104055), *UAS-Abi-RNAi* (9749R-3), and *msn-YFP* (115454) (Lye et al., 2014) are from the *Drosophila* Genetic Resource Center in Kyoto. *sqh-GFP* (318484) is from the Vienna *Drosophila* Resource Center (Sarov et al., 2016). *fat2* mosaic epithelia were produced using *FRT80B* with *e22c-Gal4* driving FLP recombinase expression. The $fat2^{N103-2}$ and $fat2^{G58-2}$ alleles were used interchangeably and are indicated in the figure legend. $Lar^{13.2}$ and $SCAR^{k13811}$ mosaic epithelia were produced using *FRT40A* with *T155-Gal4* driving FLP recombinase expression. For flipout clones, *UAS-RNAi* lines were crossed to flies with FLP recombinase under a heat shock promoter and either an *Act5c>>Gal4, UAS-RFP* or *Act5c>>Gal4, UAS-GFP* flipout cassette. Heat shock was induced by incubating pupae and adults at 37C for 1 h followed by an 11 h recovery period at 25C; this cycle was repeated 4-6 times. Females were aged on yeast overnight and dissected the next day.

Clone Labeling Method

To label mosaic epithelia in a consistent way throughout the paper, control cells are presented in cyan. In some experiments (e.g., those involving flipout clones), the manipulated cells express a clone marker. For these experiments, we applied a cyan mask during figure preparation to pseudocolor control cells instead of mutant cells. Instances of this pseudocoloring are noted in the figure legends. Additionally, control cells are labeled as "wild-type cells". In some cases, these cells represent a mixture of homozygous wild-type cells and cells that are heterozygous for the mutation being studied. We have never observed a phenotype in heterozygous cells and thus labeled the control cells "wild-type" based on their phenotype.

Time-Lapse Image Acquisition and Microscopy

One- to three-day-old females were aged on yeast with males for 1-2 days (control and *Lar* mutants) or overnight (*fat2* mutants) before dissection. Ovaries were dissected as previously described (Prasad et al., 2007) in live imaging media (Schneider's *Drosophila* medium containing 15% FBS and 200 μg/mL insulin) containing CellMask Deep Red Plasma Membrane Stain (ThermoFisher; 1:1000). Ovarioles were transferred to an agar pad (live imaging media with 0.4% NuSieve GTG low-melt agarose) formed on a gas permeable membrane slide (Sarstedt x-well) (Cetera et al., 2016). A 30 mm coverslip was placed on top of the sample, stabilized with silicon vacuum grease at each corner, and gently compressed. Halocarbon oil 27 (Sigma) was added around the coverslip to prevent evaporation. Egg chambers were imaged with a 40x 1.3 NA PlanApo objective on a laser-scanning confocal miscroscope (Zeiss LSM 880) controlled by LSM acquisition software. Time-lapse movies were performed for 10-20 minutes for control epithelia and 20-40 minutes for mutant epithelia. Single confocal slices were acquired near the basal epithelial surface every 20-30 seconds. To measure epithelial migration rates, kymographs were generated from time-lapse image stacks in Fiji (ImageJ) using the KymoResliceWide plugin (see Figure S1A for details). At least 5 egg chambers of each stage were measured.

Fixed Image Acquisition and Microscopy

Ovaries were dissected as above in live imaging media. Ovarioles were manually removed from the surrounding muscle sheath, and stage 10 and older egg chambers were discarded. We have found that this procedure greatly enhances both phalloidin and antibody staining in the follicular epithelium. Egg chambers were then fixed for 15 min in PBT (PBS + 0.1% Triton X-100) containing 4% EM-grade formaldehyde (Polysciences). For actin staining, egg chambers were incubated for 15 min in PBT with rhodamine phalloidin (Sigma, 1:200) or overnight with AlexaFluor-647 phalloidin (Invitrogen, 1:100), then washed three times in PBT. For antibody staining, egg chambers were fixed as above, washed three times in PBT, and then incubated overnight at 4C in PBT with antibody. Egg chambers were then washed three times in PBT, incubated 2-3 h at room temperature in PBT containing AlexaFluor-488 or -555-conjugated secondary antibodies (Invitrogen, 1:200), and then washed three times in PBT. After final washes, excess PBT was removed from the tissue, replaced with one drop of SlowFade Antifade (Invitrogen), then mounted onto a slide with a 50 mm coverslip. Anti-Lar (9D82B3, 1:200 concentrate), anti-Dlg (4F3, 1:20 supernatant), and anti-NCad (DN-Ex #8, 1:20 supernatant) are from the Developmental Studies Hybridoma Bank. Anti-acetylated-α-tubulin (used at 1:50) is from Santa Cruz Biotechnology. DAPI (Sigma) was added during the final wash step at 1 μg/mL. Fixed egg chambers were imaged with a laser-scanning confocal microscope (Zeiss LSM 510 or 880) using 40x 1.3 NA PlanApo and 63x 1.4 NA PlanApo objectives. For all images, a single confocal slice is shown.

Follicle Cell Primary Cultures

Ovaries from approximately 10 females were dissected in live imaging media and manually removed from the muscle sheath. Stage 11 and older egg chambers were discarded. Egg chambers were incubated in 2 mg/mL collagenase (Sigma #C6885) for 10 min at room temperature. The tissue was disrupted by vigorous pipetting, followed by several passes through a 27 gauge needle. Cells were pelleted by centrifugation (30 second at 300 x g), washed twice in live imaging media, resuspended in 100-200 μL live imaging media, and plated onto concanavalin-A-coated 22 mm coverslips for 30 min. Cells were then fixed for 10 min in PBS containing 4% formaldehyde, and washed several times in PBS. Immunostaining with anti-Lar and anti-GFP antibodies was performed sequentially to allow both non-permeabilized staining of Lar and permeabilized staining of GFP. Cells were incubated for 1 hour with anti-Lar antibody (1:500 in PBS), washed several times in PBS, and then incubated for 30 min in AlexaFluor-647 secondary antibody (Invitrogen, 1:400 in PBS). After several more washes in PBS, cells were again fixed for 10 min in PBS containing 4% formaldehyde, washed several times in PBS, and then permeabilized for10 min in PBT. After permeabilization, cells were incubated 1 hour with AlexaFluor-488-conjugated GFP antibody (Invitrogen, 1:1000 in PBT), and then washed in PBT. Cells were then incubated 10 min in PBT with rhodamine phalloidin (1:1000), and washed several times in PBT. DAPI was added during the final wash step at 1 μg/mL. Coverslips were mounted to a microscope slide in SlowFade Antifade. Cells were imaged with a laser-scanning confocal microscope (Zeiss LSM 800) using a 63x 1.4 NA PlanApo objective. All images represent a single confocal slice.

Quantification of Protrusions

Analysis was performed on stage 7 mosaic epithelia stained with phalloidin as described above. Epithelia analyzed met two additional criteria: 1) the stress fibers in every cell were oriented perpendicular to the egg chamber's anterior-posterior (A-P) axis, and 2) protrusions in wild-type cells appeared normal compared to non-mosaic controls. The latter criterion was used to exclude epithelia whose protrusions were not well preserved through the dissection and fixation protocols. Individual cells were scored by eye and binned into one of three groups (normal, weak, or none) based on comparison to control non-mosaic epithelia. A cell was determined to have weak protrusions if they were reduced in either number or intensity. In control mosaics, both GFP-expressing and non-GFP-expressing cells at clone boundaries were scored. Graphs indicate which cells were scored in mosaic epithelia.

Quantification of Fat2 and Lar Colocalization

Lar was visualized by antibody staining in either stage 7 *fat2-3xGFP* epithelia or *fat2$^{\Delta ICD}$-3xGFP* mosaic epithelia. Line scans were generated manually in ImageJ; a 10-pixel wide line was drawn over cell membranes that are roughly parallel to the egg chamber's A-P axis (yellow lines in Figures S3A and S4D). GFP or Lar fluorescence intensity values for each point along the line were obtained with the Plot Profile function, and then plotted against each other. Pearson correlation coefficients were determined from these plots using Prism 6 (GraphPad). Each line scan covered 5-10 cell-cell interfaces. For Fat2$^{\Delta ICD}$-3xGFP, measurements were also made along cell-cell contacts perpendicular to the A-P axis (blue lines in Figure S4D). Colocalization between Fat2$^{\Delta ICD}$-3xGFP and Lar was analyzed within *fat2$^{\Delta ICD}$-3xGFP* clones.

Quantification of Fat2 and Lar Polarity

Fat2-3xGFP, Lar, and Fat2$^{\Delta ICD}$-3xGFP polarity were measured using Packing Analyzer V2 software as described (Aigouy et al., 2010). The software calculates the axis and magnitude of junctional polarity (nematic order) based on the perimeter intensity of the junctional protein. This is represented by the symmetric tensor components Q_1 and Q_2, as described (Aigouy et al., 2010). Tensor components Q_1 and Q_2 were normalized by the average boundary intensity of a given cell as described (functions 1-2, Aw et al., 2016). Cells were segmented using the Lar or Fat2 fluorescence channel after adjusting the brightness and contrast to enhance the signal in ImageJ. Errors were corrected manually using cell boundaries as defined by actin fluorescence. This segmented mask was applied to the original Lar or Fat2 fluorescence image for analysis. Data were plotted in a circular histogram (rose diagram) using the polar plot function in MATLAB. Histograms were weighted by the average magnitude of polarity within each bin to reflect the strength of polarity as described (Aw et al., 2016).

Nuclear Positioning Measurements

Analysis was performed on stage 7 mosaic epithelia. As above, epithelia were analyzed only if the stress fibers in every cell were oriented perpendicular to the egg chamber's A-P axis. Cell cortices were marked with anti-Dlg or anti-NCad and nuclei were marked using DAPI. Nuclear centroids and the positions of the leading and trailing edges were found manually in images taken at the basal surface (as determined by phalloidin staining), and distances between features were calculated in ImageJ. In $Lar^{13.2}$ and $SCAR^{k13811}$ mosaics, only wild-type cells directly ahead of mutant cells were analyzed. $SCAR^{k13811}$ mosaics were only analyzed if protrusions were completely lost in mutant cells. In $fat2^{N103\text{-}2}$, *fat2-RNAi*, $fat2^{\Delta ICD}$*-3xGFP*, and *CLASP-RNAi* mosaics, mutant cells directly behind wild-type cells were measured.

Generation of Fat2-3xGFP and Fat2$^{\Delta ICD}$-3xGFP

Generation of *fat2-3xGFP* and $fat2^{\Delta ICD}$*-3xGFP* lines was achieved using CRISPR-Cas9-mediated homologous recombination, following the general design strategies described by Gratz et al. (Gratz et al., 2013; 2014). Target sequences were cloned into the pU6-BbsI-chiRNA plasmid, which contains the *Drosophila* snRNA:U6:96Ab promoter for in vivo transcription. For *fat2-3xGFP*, the target sequence selected for gRNA production was 5'-GAGGGGCCGATTTCTAGGA**TGG**-3'. For $fat2^{\Delta ICD}$*-3xGFP*, this target sequence was used in combination with a second target sequence: 5'-GAACAAGTCGTCGTACAAGG**AGG**-3'. Underlined sequences were cloned into pU6-BbsI-chiRNA; adjacent PAM motifs are shown in bold.

"Donor" plasmids for homologous recombination were engineered to contain three tandem copies of GFP coding sequence (3xGFP) followed by a floxed 3xP3-DsRed module (Gratz et al., 2014) for screening potential insertion events. Flanking this 3xGFP-3xP3-DsRed cassette were ~2 kb homology arms containing sequence matching that on either side of the target locus. For *fat2-3xGFP*, 3xGFP sequence was inserted after position 19,182 in the *fat2* gene (20,024,482 in the *Drosophila* genome). This corresponds to amino acid 4689 of the Fat2 protein (according to the isoform C sequence). For $fat2^{\Delta ICD}$*-3xGFP*, bases 17,382 to 19,182 in the *fat2* gene (20,022,682 to 20,024,482 in the *Drosophila* genome) were replaced with 3xGFP sequence. This corresponds to the 3xGFP tag being inserted following amino acid 4321.

Injections were performed in-house. A mixture of dsDNA donor plasmid (300 ng/μL) and plasmid(s) encoding gRNAs (50 ng/μL) was injected into *vas-Cas9;; FRT80* embryos. *vas-Cas9* flies were generously provided by Yi Guo (Sebo et al., 2014). Because the *vas-Cas9* insertion was marked with both 3xP3-GFP and 3xP3-RFP, we used *vas-Cas9* flies in which the RFP sequence had been previously mutated by gRNA targeting (Sebo et al., 2014). Resulting adults were crossed to balancer flies. Founders were identified in the progeny of this cross by DsRed expression in the adult eye using a Leica MZ FL III microscope; these founders were used to establish stocks. After insertions were verified by sequencing, founder lines were crossed to *Cre*-expressing flies to excise the DsRed module. Four independent *fat2-3xGFP* lines and three independent $fat2^{\Delta ICD}$*-3xGFP* lines were established; we observed no differences between independently-derived lines for either genotype. Full sequences of donor plasmids are listed in Data S1.

Quantification of Egg Aspect Ratio

Ovaries were dissected in freshly made 50% Robb's minimal saline, and then fixed in 50% Robb's containing 8% formaldehyde for 5 min. The tissue was disrupted by vigorous pipetting to remove muscle sheath, then plated onto a microscope slide in minimal buffer, covered with a coverslip, and immediately imaged on an upright compound microscope (Leica DM550B) using a 10x air objective. Stage 14 egg chambers and mature eggs were analyzed. Aspect ratios were calculated by dividing egg (chamber) length by width in ImageJ; dorsal appendages were not included in measurements.

Quantification of Sqh-GFP Fluorescence

Analysis was performed in ImageJ. Fluorescent images were obtained with identical microscope settings across genotypes, and identical intensity thresholds were applied. Thresholded images were then made binary, and relative fluorescence was calculated by dividing the number of pixels in a manually-chosen region of interest by the total area of the same region. For *fat2* mosaics, only *fat2* null cells were analyzed.

QUANTIFICATION AND STATISTICAL ANALYSIS

All data were obtained from at least two independent experiments, and several females were analyzed each time. All data were highly reproducible. No statistical method was used to predetermine sample size. The samples size for most experiments can be found either on the figure panel or within the figure legend, and the statistical test used and dispersion/precision measures are in the figure legends. The one exception is the data presented in Figure 2D. For these data the statistical information is presented in Table S1. As listed, either a Student's t-test or one-way ANOVA was used to determine whether data from two experimental conditions were significantly different, and this analysis was performed using Prism software (Graph Pad). These tests are appropriate because all data obtained follow an approximately normal distribution. Differences between experimental and control conditions were large in all cases and the variability within a single experimental condition was typically low. Pearson's coefficients were obtained by correlation analysis performed using Prism, and pools of Pearson's coefficients were compared by a Student's t-test. The experiments were not randomized, nor was the data analysis performed blind. Egg chambers damaged by the dissection process were excluded from analysis.

Inventory of Supplemental Information

Figure S1, related to Figures 2 and 3, Background on three methods used in this paper
Figure S2, related to Figure 2, Fat2 and Lar are planar polarized from early stages
Figure S3, related to Figure 4, Further characterization of Fat2's and Lar's localization
Figure S4, related to Figure 6, Fat2's ECD stabilizes Lar and induces protrusions
Figure S5, related to Figure 6, Fat2 stabilizes Lar in follicle cell clusters
Figure S6, related to Figure 7, Nuclear position elucidates trailing edge retraction defects
Figure S7, related to Figure 7, Ruling out models for Fat2's role in trailing edge retraction

Movie S1, related to Figure 2, Lar promotes the migration of the follicular epithelium

Table S1, related to Figure 2, Sample sizes and P-values for migration rate measurements
Table S2, related to STAR Methods, Detailed experimental genotypes

Excel spreadsheet S1, related to STAR Methods, Donor plasmid sequences

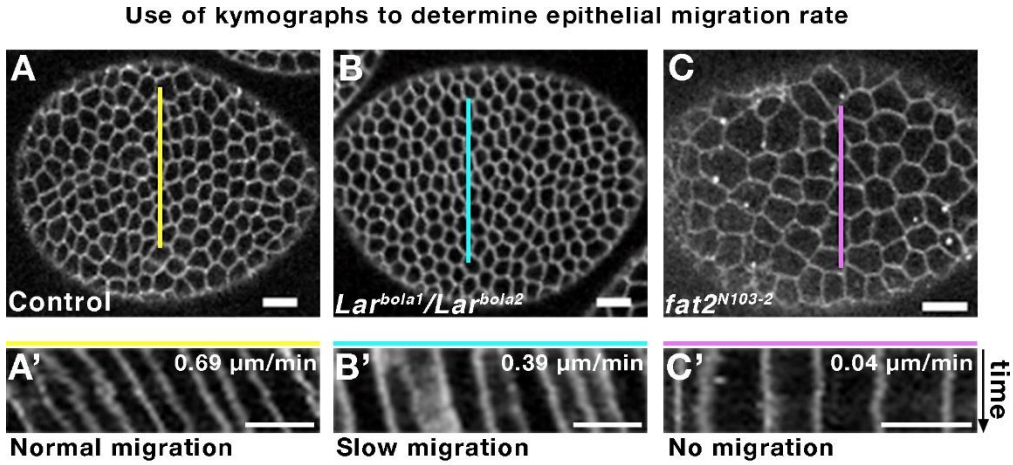

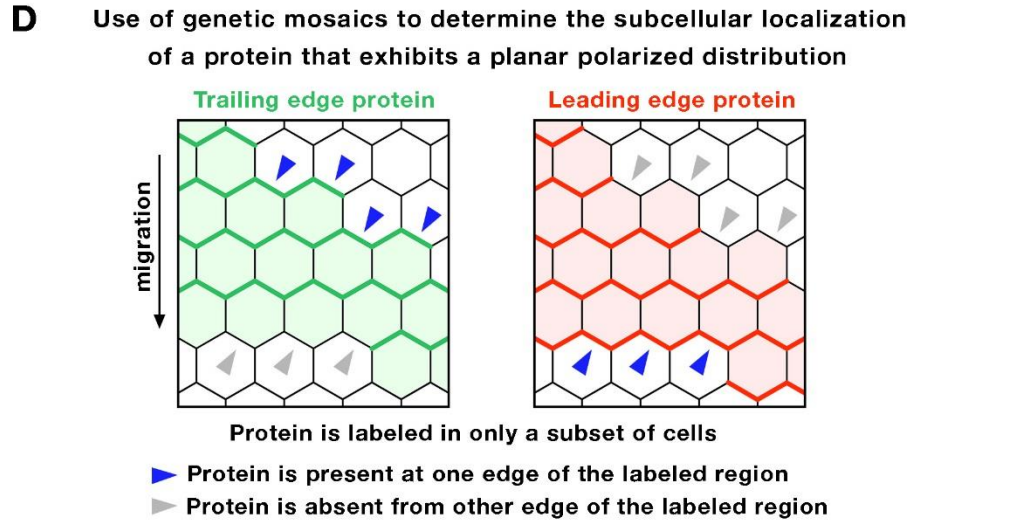

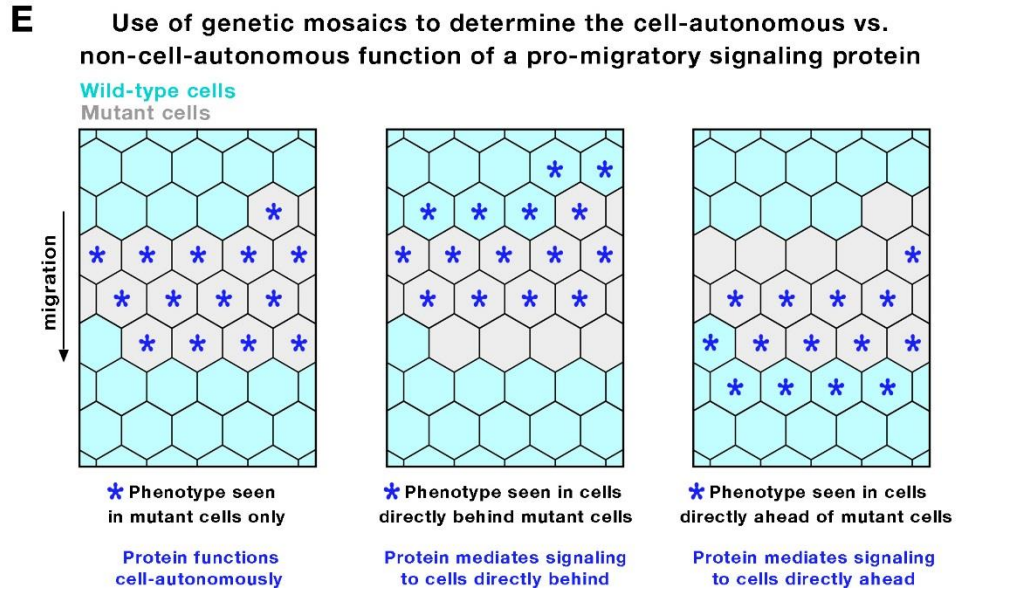

Barlan et al., Figure S1

Figure S1. Background on three methods used in this paper, Related to Figures 2 and 3.
(A-C) Use of kymographs to determine epithelial migration rates. The examples shown represent control (A), *Lar* null (B) and *fat2* null (C) epithelia at stage 6 that have been stained with CellMask to mark plasma membranes. In the top panels, the colored lines mark the position on the epithelium from which the kymograph was generated. In the bottom panels (A'-C'), the colored lines have been rotated 90 degrees and the images (kymographs) show how the positions of the intersecting cell membranes change over the course of a 10 minute movie. Migration rates are calculated by measuring the slope of 3-4 lines in each kymograph and averaging those values. Scale bars, 10 μm.
(D and E) Use of genetic mosaics to identify the subcellular localization of protein that shows a planar polarized distribution (D) and the cell-autonomous vs. non-cell-autonomous function of a pro-migratory signaling protein (E). Illustrations represent the basal surface of the follicular epithelium. When mosaic analyses are performed on fixed tissue, the direction of migration is determined by the orientation of the leading edge protrusions across the epithelium. Protrusions are not depicted on the illustrations.

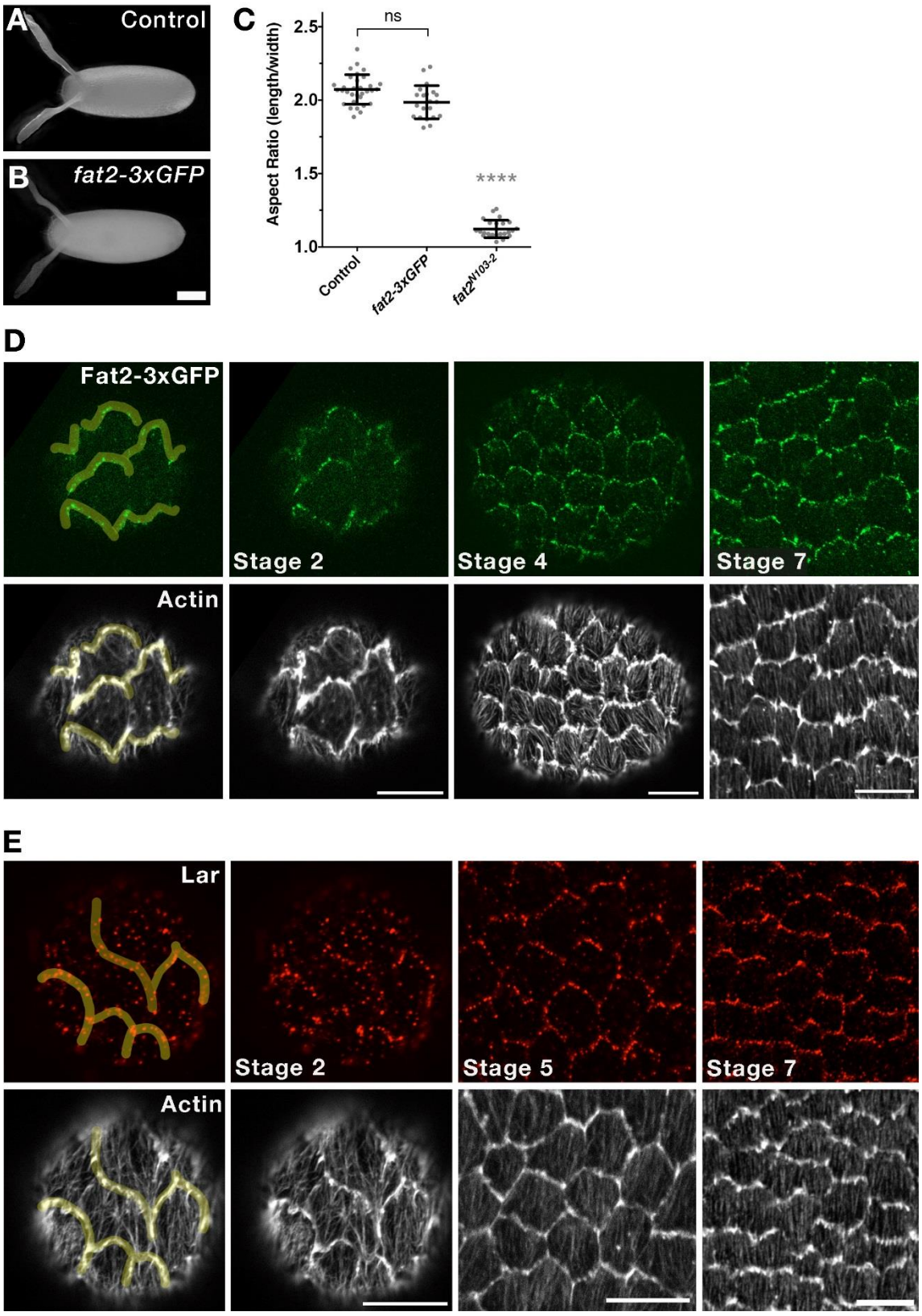

Barlan et al., Figure S2

Figure S2. Fat2 and Lar are planar polarized from early stages, Related to Figure 2.
(A-C) *fat2-3xGFP* is a functional transgene. (A and B) Representative images of control (A) and *fat2-3xGFP* (B) eggs. Scale bar, 100 µm. (C) Aspect ratios of stage 14 and mature eggs, determined by dividing egg length by width, show that *fat2-3xGFP* egg shape is not significantly different than controls, but is significantly different from a *fat2* null condition. Individual data points; mean ± SD. One-way ANOVA: **** $p \leq 0.0001$. *n* = 32 eggs for control; *n* = 21 eggs for *fat2-3xGFP; n* = 24 eggs for $fat2^{N103\text{-}2}$.
(D and E) Fat2-3xGFP (D) and Lar (E) localization at the basal epithelial surface at three different developmental stages. In leftmost panels, stage 2 images have been overlaid with yellow traces to highlight interfaces between neighboring cells' leading and trailing edges. Both proteins are planar polarized at cell-cell interfaces at latest by stage 2. Scale bars, 10 µm. Images in (D) and (E) are oriented such that the direction of migration is down.

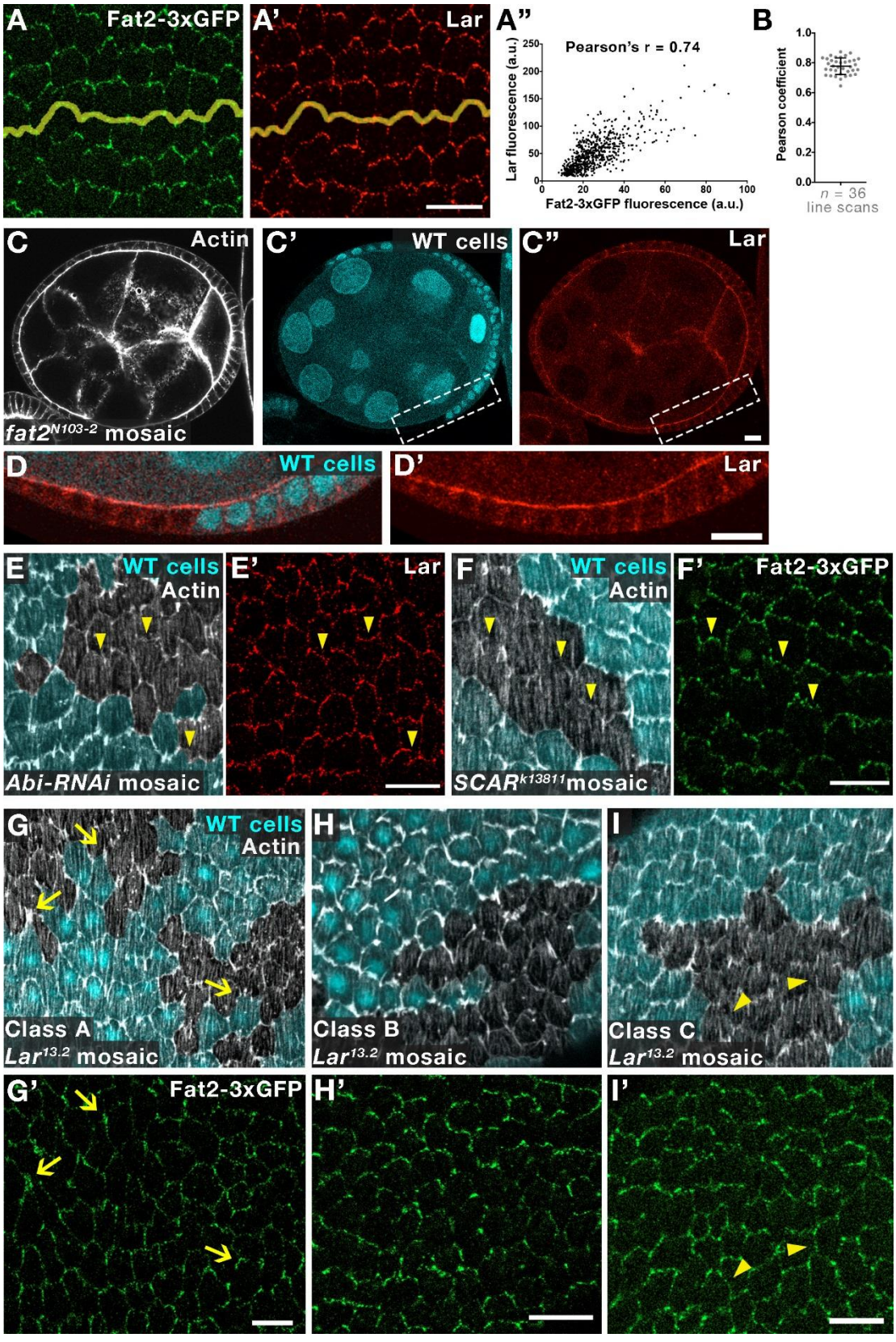

Barlan et al., Figure S3

Figure S3. Further examination of Fat2's and Lar's localization, Related to Figure 4.

(A and B) Quantification of colocalization of Fat2 and Lar at the basal surface of the follicular epithelium. Lar was visualized by antibody staining in *fat2-3xGFP* epithelia (A, A'). Line scans were generated manually by tracing cell-cell interfaces (yellow lines). For each point along the line, GFP and Lar fluorescence values were plotted against one another. Plot shown in (A'') corresponds to images in (A, A'). Pearson correlation coefficients calculated from multiple line scan analyses in *fat2-3xGFP* epithelia are shown in (B).

(C and D) Lar levels are normal at the apical surface of $fat2^{N103\text{-}2}$ follicle cells. (C-C'') Central sagittal section through a $fat2^{N103\text{-}2}$ mosaic egg chamber. Boxed regions are blown up in (D, D').

(E and F) Localization of Lar in a clone of cells expressing *Abi-RNAi* (E) and Fat2-3xGFP in a $SCAR^{k13811}$ mosaic epithelium, both of which lose protrusions in a cell-autonomous manner (triangles). These data show that protrusions are not required for Lar's leading edge localization, and that both proteins can localize normally in small clones of non-migratory cells that are carried along by their wild-type neighbors. Wild-type cells in (E) are pseudocolored cyan.

(G-I) Loss of Lar has weak and variable effects on Fat2 localization. Representative basal surface images from three classes of Fat2-3xGFP localization phenotypes observed in $Lar^{13.2}$ mosaic epithelia. In all cases, Fat2-3xGFP remains on the plasma membrane, but shows slight defects in its localization. In Class A (G, G'), Fat2-3xGFP appears slightly enriched in the trailing edge extensions of wild-type cells positioned directly ahead of $Lar^{13.2}$ cells (arrows). In Class B (H, H'), Fat2-3xGFP intensity appears slightly reduced in $Lar^{13.2}$ cells. In Class C (I, I'), Fat2-3xGFP appears less planar polarized within the $Lar^{13.2}$ clone. Triangles in (I') show Fat2-3xGFP aberrantly localized along lateral cell edges.

Images in (A) and (E-I) are oriented such that the direction of migration is down. All experiments are at stage 7. Scale bars, 10 μm.

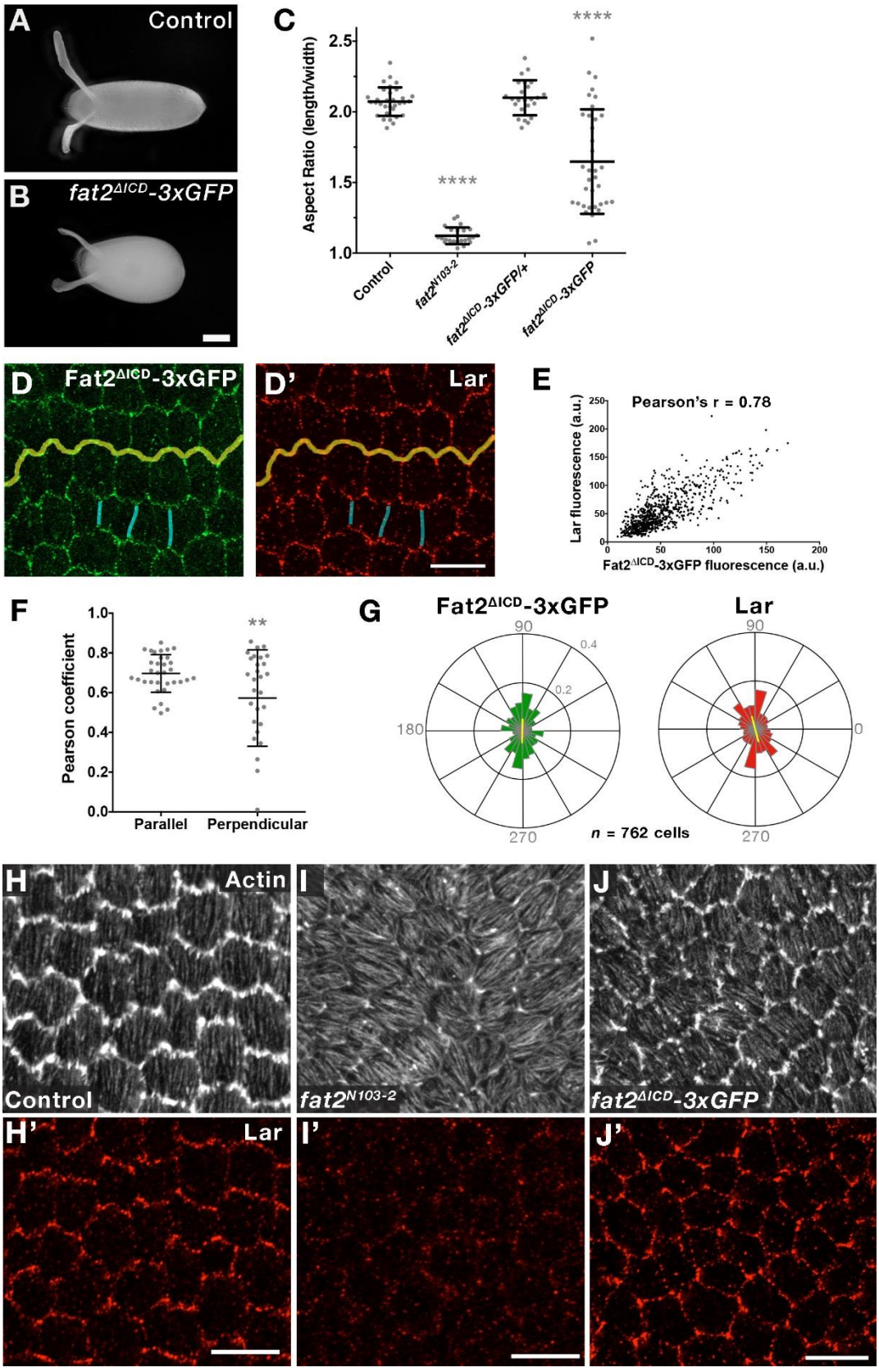

Barlan et al., Figure S4

Figure S4. Fat2's ECD stabilizes Lar and induces protrusions, Related to Figure 6.

(A-C) Eggs from *fat2*$^{\Delta ICD}$*-3xGFP* females have variable elongation defects. Representative images of control (A) and *fat2*$^{\Delta ICD}$*-3xGFP* eggs (B). Scale bar, 100 µm. (C) Aspect ratios (length/width) of stage 14 egg chambers/eggs, show that many *fat2*$^{\Delta ICD}$*-3xGFP* eggs are rounded, but they are rarely as round as *fat2*$^{N103-2}$ eggs. This effect is not observed in *fat2*$^{\Delta ICD}$*-3xGFP* heterozygotes. Control and *fat2*$^{N103-2}$ data shown in (C) are the same as in Figure S2C. Individual data points; mean ± SD. One-way ANOVA: **** $p \leq 0.0001$. *n* = 32 eggs for control; *n* = 24 eggs for *fat2*$^{N103-2}$; *n* = 24 eggs for *fat2*$^{\Delta ICD}$*-3xGFP*/+; *n* = 36 eggs for *fat2*$^{\Delta ICD}$*-3xGFP*.

(D-F) Quantification of colocalization of Fat2$^{\Delta ICD}$-3xGFP and Lar at the basal surface of stage 7 *fat2*$^{\Delta ICD}$*-3xGFP* mosaic epithelia. Line scans were generated manually by tracing cell-cell interfaces parallel to the AP axis (yellow lines) and perpendicular to the AP axis (blue lines). For each point along the lines, GFP and Lar fluorescence values were plotted against one another. Plot in (E) corresponds to the yellow line in (D, D'). Pearson correlation coefficients calculated from multiple line scans in *fat2*$^{\Delta ICD}$*-3xGFP* mosaic epithelia are shown in (F). Unpaired t-test: ** $p \leq 0.01$. *n* = 33 parallel line scans; *n* = 29 perpendicular line scans. Image in (D, D') is a *fat2*$^{\Delta ICD}$*-3xGFP* clone within a mosaic epithelium. Scale bar, 10 µm.

(G) Rose diagrams showing that Fat2 and Lar are less well planar polarized in *fat2*$^{\Delta ICD}$*-3xGFP* epithelia than in control epithelia (compare with Figure 5C). 10 egg chambers were analyzed. Yellow lines indicate average angle and magnitude of polarity.

(H-J) Comparison of protrusion formation and Lar localization at the basal surface of control (H, H'), homozygous *fat2*$^{N103-2}$ (I, I'), and homozygous *fat2*$^{\Delta ICD}$*-3xGFP* (J, J') epithelia at stage 7. In both *fat2*$^{N103-2}$ and *fat2*$^{\Delta ICD}$*-3xGFP* epithelia, tissue-level stress fiber alignment is disrupted, likely due to a defect in migration. However, unlike *fat2*$^{N103-2}$ epithelia where protrusions and Lar are both largely missing from the basal surface, these features are both present in *fat2*$^{\Delta ICD}$*-3xGFP* epithelia. Lar fluorescence images were obtained with identical microscope settings. Scale bars, 10 µm.

Images in (D) and (H) are oriented such that the direction of migration is down. Images in (I) and (J) are oriented such that the egg chamber's posterior is to the right.

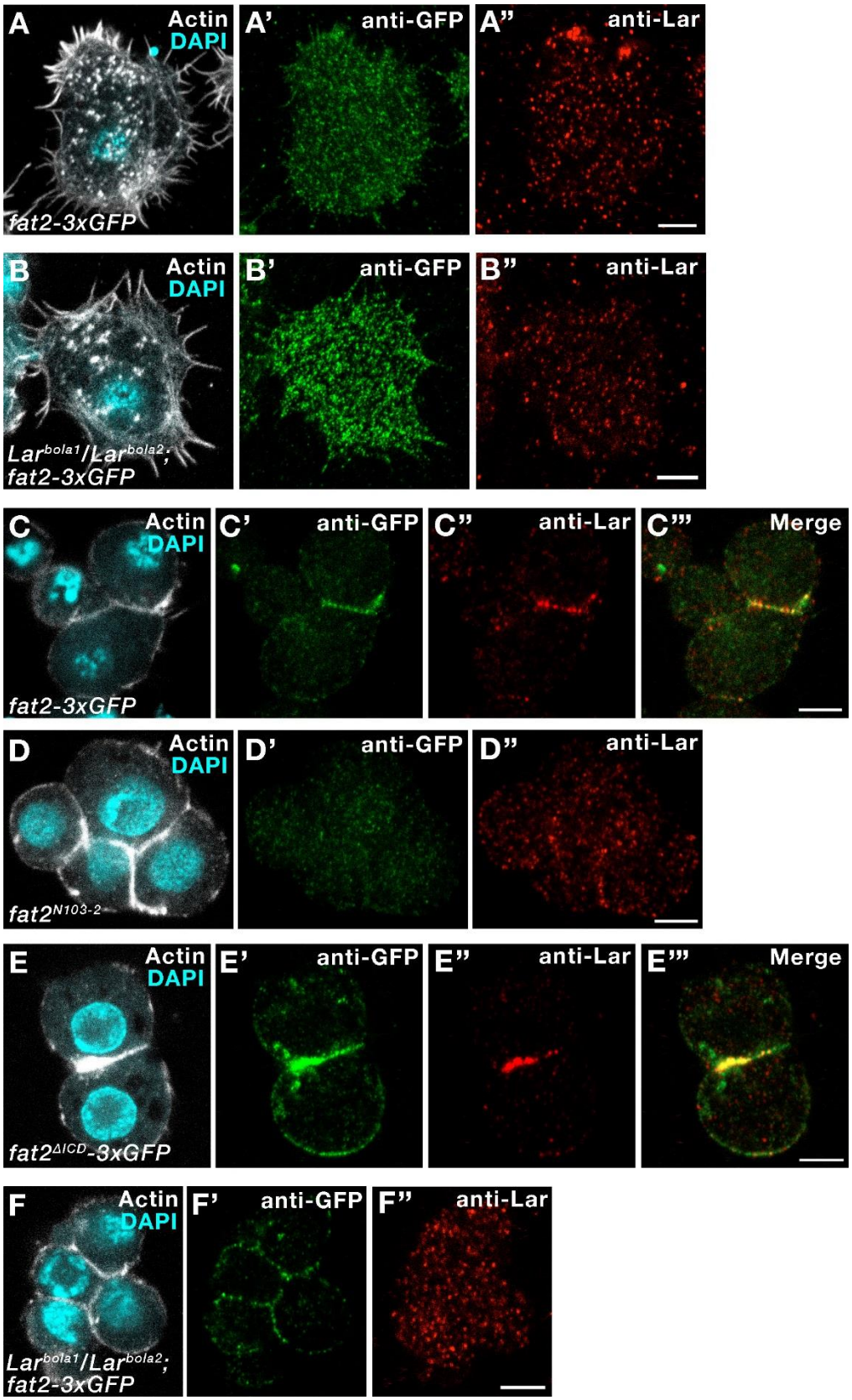

Barlan et al., Figure S5

Figure S5. Fat2 stabilizes Lar in follicle cell clusters, Related to Figure 6.

(A and B) Representative images of individual follicle cells expressing Fat2-3xGFP that were isolated by dissociating either control (A) or *Lar* null epithelia (B). Although Fat2-3xGFP forms puncta in these cells, Lar protein is largely undetectable. Comparing the red channel between the control and *Lar* null cells indicates that the staining observed with the Lar antibody under these conditions is largely non-specific. Images were obtained with identical microscope settings.

(C) In a cluster of dissociated control follicle cells, Lar can be seen colocalizing with Fat2-3xGFP at cell-cell interfaces.

(D) In a cluster of dissociated *fat2* null follicle cells, Lar localization at cell-cell interfaces is strongly reduced.

(E) In a cluster of dissociated *fat2*$^{\Delta ICD}$*-3xGFP* follicle cells, Lar continues to colocalize with Fat2$^{\Delta ICD}$-3xGFP at cell-cell interfaces, showing that Fat2's ICD is not required to stabilize Lar at cell-cell contacts.

(F) In a cluster of dissociated *Lar* null follicle cells, Fat2-3xGFP continues to be enriched at cell-cell interfaces.

Images in (C-F) were obtained with identical microscope settings. Scale bars, 5 μm.

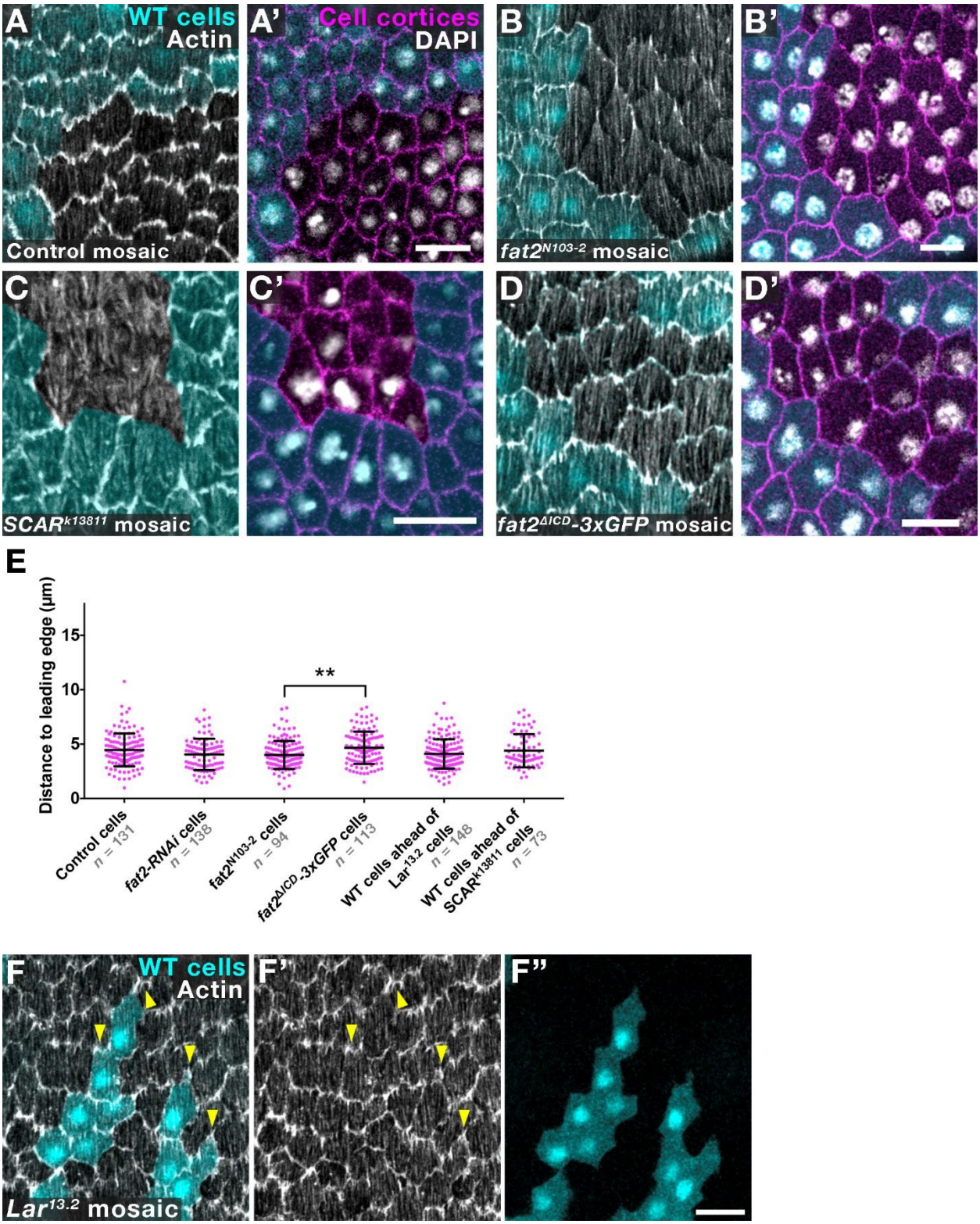

Barlan et al., Figure S6

Figure S6. Nuclear position elucidates trailing edge retraction defects, Related to Figure 7.
(A-D) Representative images of trailing edge retraction defects. Stage 7 mosaic epithelia stained with anti-Dlg to label cell cortices and DAPI to label nuclei. (A) Cells in control mosaics have nuclei that are roughly equidistant from the leading and trailing edges. In *fat2*$^{N103\text{-}2}$ cells in mosaic epithelia (B), the distance between the nucleus and the cell's trailing edge increases. A moderate trailing edge extension phenotype is present in the wild-type cells directly ahead of *SCAR*^{k13811} cells (C), suggesting that protrusions help to release the trailing edge of the cell in front. A moderate extension of the trailing edge is also seen in *fat2*$^{\Delta ICD}$*-3xGFP* cells (D), suggesting that Fat2's ICD may transduce a signal necessary for retraction. Wild-type cells in (C and D) are pseudocolored cyan. Scale bars, 10 μm.
(E) Quantification of the distance between nucleus and leading edge, measured at the basal surface of stage 7 mosaic epithelia. In *Lar*$^{13.2}$ and *SCAR*^{k13811} mosaics, measurements were made on wild-type cells directly in front of mutant cells. In other conditions, measurements were made on mutant cells themselves. In elongated cells, the trailing edge extension gives the appearance that nuclei are closer to the leading edge than in controls. However, measuring the distance between nucleus and leading edge in these cells reveals no significant change compared to cells in control mosaics (A). Comparing *fat2*$^{N103\text{-}2}$ and *fat2*$^{\Delta ICD}$*-3xGFP* cells shows a small but statistically significant difference in the distance between nucleus and leading edge (asterisks), but a much larger difference between nucleus and trailing edge (see Figure 7D). Individual data points, mean ± SD. One-way ANOVA: ** $p \leq 0.01$.
(F) Images showing that wild-type cells directly ahead of *Lar* null cells have extended trailing edges even when protrusions are still present on the *Lar* cells (yellow arrowheads). Thus, Lar plays a signaling role in stimulating trailing edge retraction that is independent of its role in protrusion formation. Scale bars, 10 μm.

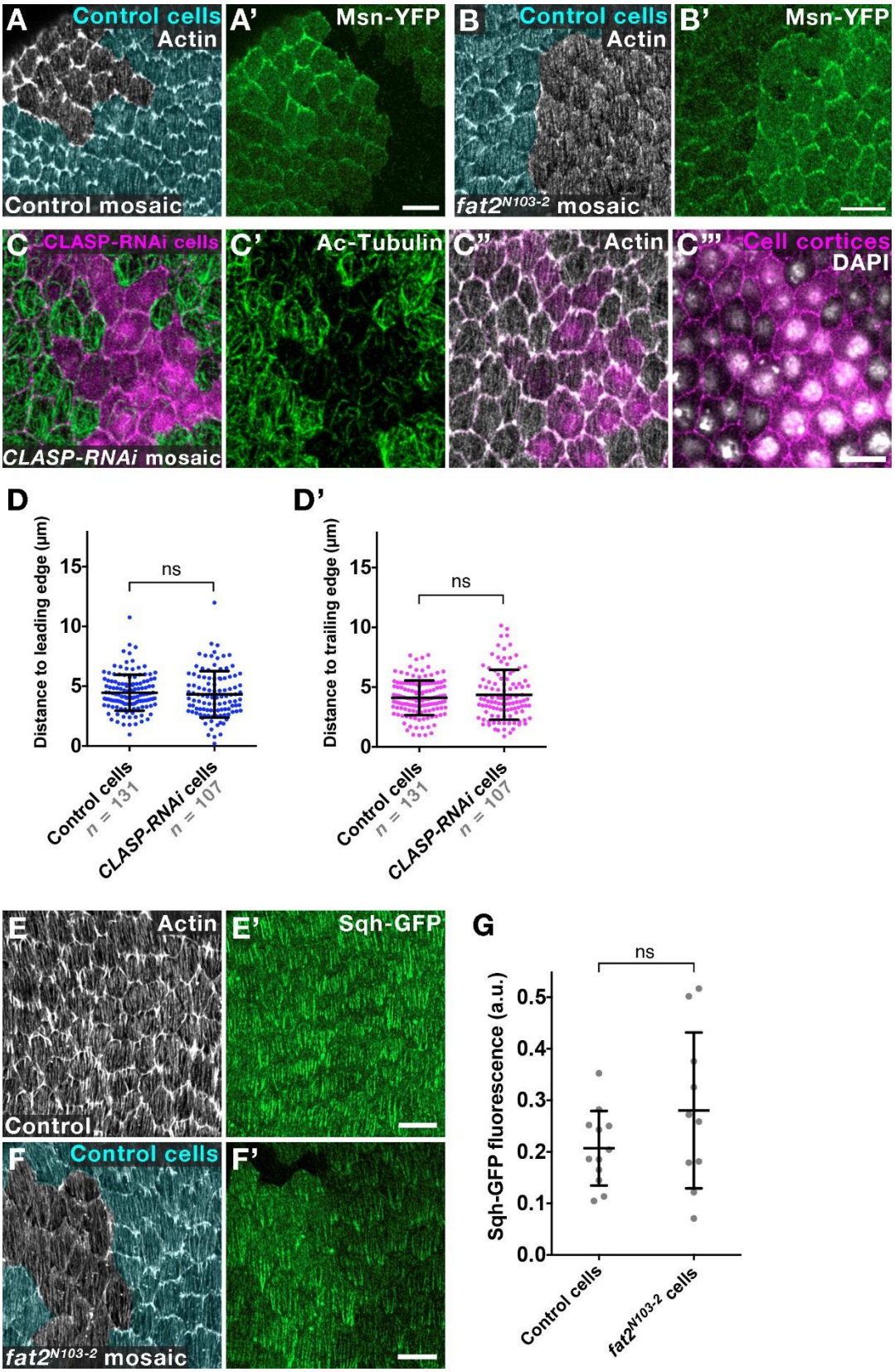

Barlan et al., Figure S7

Figure S7. Ruling out models for Fat2's role in trailing edge retraction, Related to Figure 7.
(A and B) Representative images showing that Msn localization is equivalent between control (A, A') and *fat2* null mosaic epithelia. Control cells are pseudocolored cyan. In (A') and (B') any given cell can have either 0, 1, or 2 copies of the Msn-YFP protein trap. Comparisons should be made on cells that lack the cyan clone marker in (A) and (B); these are labelled with two copies of Msn-YFP.
(C and D) CLASP is not required for trailing edge retraction. Stage 7 *CLASP-RNAi* mosaic epithelium stained with anti-NCad to label cell cortices and DAPI to label nuclei. (C-C''') Images showing that *CLASP-RNAi* cells do not have elongated basal surfaces. The effectiveness of the RNAi is evidenced by the strong reduction of microtubules at the basal surface of the clone. (D, D') Quantification of the dataset represented in (C), measuring the distance between the nucleus and either the cell's leading (D) or trailing edge (D'). Control data in (D, D') is the same as that shown in Figure 7D and Figure S6E.
(E-G) Myosin recruitment to stress fibers is normal in *fat2* null cells. (E and E') Representative images of the basal surface of a wild-type epithelium expressing 2 copies of a fosmid in which the myosin regulatory light chain Spaghetti squash (Sqh) is tagged with GFP. (F and F') Representative images of a *fat2* mosaic epithelium in which a given cell can express either 0, 1, or 2 copies of Sqh GFP. *fat2* null cells that lack the cyan clone marker always express 2 copies of Sqh-GFP which is used for comparison with the control cells in (E). (G) Quantification of the data represented by (E) and (F). n = 12 control egg chambers; n = 10 *fat2* mosaic egg chambers.
All experiments performed at stage 7. Scale bars, 10 μm.

Movie S1. Lar promotes the migration of the follicular epithelium, Related to Figure 2.
(A-D) Time-lapse sequences of migration in stage 6 epithelia. Cell membranes are labeled, and images are taken close to the basal epithelial surface. (A) A control (w^{1118}) epithelium migrating at a rate of 0.65 µm/min. (B) A Lar^{bola1}/Lar^{bola2} epithelium migrating slowly at 0.39 µm/min. (C) A non-migratory (0.065 µm/min) Lar^{bola1}/Lar^{bola2} epithelium. (D) A non-migratory (0.015 µm/min) $fat2^{N103\text{-}2}$ epithelium. An epithelium is deemed "non-migratory" if its migration rate is less than or equal to the fastest rate obtained for a $fat2^{N103\text{-}2}$ epithelium, as *fat2* null epithelia have been have previously been established never to migrate (Cetera et al., 2014; Chen et al., 2016). Sequences are 40 frames; elapsed time is displayed in minutes. Scale bars, 20 µm.

Table S1. Sample sizes and P-values for migration rate measurements, Related to Figure 2.

P-values were generated using unpaired t-tests between the conditions listed.

Stage	**Control**	***Lar*^{bola1}/*Lar*^{bola2}**	***fat2*$^{N103-2}$**	**Control vs *Lar*^{bola1}/*Lar*^{bola2}**	***Lar*^{bola1}/*Lar*^{bola2} vs *fat2*$^{N103-2}$**
1	*n* = 5	*n* = 5	*n* = 5	P = 0.1344	P = 0.0035
2	*n* = 7	*n* = 7	*n* = 9	P = 0.0006	P = 0.0117
3	*n* = 7	*n* = 13	*n* = 11	P = 0.0007	P = 0.0572
4	*n* = 13	*n* = 13	*n* = 11	P <0.0001	P = 0.0622
5	*n* = 10	*n* = 14	*n* = 11	P = 0.0002	P = 0.0178
6	*n* = 14	*n* = 13	*n* = 6	P <0.0001	P = 0.0427
7	*n* = 8	*n* = 6	*n* = 5	P <0.0001	P = 0.3396

Table S2. Detailed experimental genotypes, Related to STAR methods.

Figure	Panel	Genotype
1	H, I	*w;; fat2-3xGFP, FRT80*
2	A	w^{1118}
	B, C	Lar^{bola1}/Lar^{bola2}
	D	w^{1118} Lar^{bola1}/Lar^{bola2} $w;; fat2^{N103-2}$, *FRT80*
	E	*hsFlp/+;; Act5c>>Gal4, UAS-GFP/UAS-Lar-RNAi*$^{TRiP.GL01589}$
	F	*e22c-Gal4, UAS-Flp/+; fat2-3xGFP, FRT80/ mRFP-nls, FRT80*
3	A	*e22c-Gal4, UAS-Flp/+; ubi-eGFP, FRT80/FRT80*
	B	$Lar^{13.2}$*, FRT40/ubi-mRFP-nls, FRT40; T155-Gal4, UAS-Flp/+*
	C	*e22c-Gal4, UAS-Flp/+;* $fat2^{N103-2}$*, FRT80/ubi-eGFP, FRT80*
	D-F	*e22c-Gal4, UAS-Flp/+;* $fat2^{G58-2}$*, FRT80/ubi-eGFP, FRT80*
	G	*e22c-Gal4, UAS-Flp/+; ubi-eGFP, FRT80/FRT80* $Lar^{13.2}$*, FRT40/ubi-mRFP-nls, FRT40; T155-Gal4, UAS-Flp/+* *e22c-Gal4, UAS-Flp/+;* $fat2^{N103-2}$*, FRT80/ubi-eGFP, FRT80*
4	A-C	*w;; fat2-3xGFP, FRT80*
	D	*e22c-Gal4, UAS-Flp/+;* $fat2^{N103-2}$*, FRT80/ubi-eGFP, FRT80*
5	A, B	*tj-Gal4/+; fat2-3xGFP, FRT80/UAS-Abi-RNAi*$^{DGRC9749R-3}$
	C	*w;; fat2-3xGFP, FRT80*
	D	*tj-Gal4/+; fat2-3xGFP, FRT80/UAS-Abi-RNAi*$^{DGRC9749R-3}$
6	A	*e22c-Gal4, UAS-Flp/+;* $fat2^{\Delta ICD}$*-3xGFP, FRT80/FRT80*
	B, C	*e22c-Gal4, UAS-Flp/+;* $fat2^{\Delta ICD}$*-3xGFP, FRT80/ubi-eGFP, FRT80*
7	A	*hsFlp/+;; Act5c>>Gal4, UAS-RFP/UAS-fat2-RNAi*$^{TRiP.HMS02136}$
	B	$Lar^{13.2}$*, FRT40/ubi-eGFP, FRT40; T155-Gal4, UAS-Flp/+*
	D	*e22c-Gal4, UAS-Flp/+; ubi-eGFP, FRT80/FRT80* *hsFlp/+;; Act5c>>Gal4, UAS-RFP/UAS-fat2-RNAi*$^{TRiP.HMS02136}$ *e22c-Gal4, UAS-Flp/+;* $fat2^{N103-2}$ *FRT80/ubi-eGFP, FRT80* *e22c-Gal4, UAS-Flp/+;* $fat2^{\Delta ICD}$*-3xGFP, FRT80/ubi-eGFP, FRT80* $Lar^{13.2}$*, FRT40/ubi-mRFP-nls, FRT40; T155-Gal4, UAS-Flp/+* $SCAR^{k13811}$*, FRT40/ubi-eGFP, FRT40; T155-Gal4, UAS-Flp/+*
S1	A	w^{1118}
	B	Lar^{bola1}/Lar^{bola2}
	C	$w;; fat2^{N103-2}$*, FRT80*
S2	A	w^{1118}
	B	*w;; fat2-3xGFP, FRT80*
	C	w^{1118} *w;; fat2-3xGFP, FRT80* $w;; fat2^{N103-2}$*, FRT80*
	D	*w;; fat2-3xGFP, FRT80*
	E	w^{1118}
S3	A, B	*w;; fat2-3xGFP, FRT80*
	C, D	*e22c-Gal4, UAS-Flp/+;* $fat2^{N103-2}$ *FRT80/ubi-eGFP, FRT80*

	E	*hsFlp/+;; Act5c>>Gal4, UAS-RFP/UAS-Abi-RNAi$^{DGRC9749R-3}$*
	F	*SCAR^{k13811}, FRT40/ubi-mRFP-nls, FRT40; T155-Gal4, UAS-Flp/fat2-3xGFP, FRT80*
	G-I	*Lar$^{13.2}$, FRT40/ubi-mRFP-nls, FRT40; fat2-3xGFP, FRT80/T155-Gal4, UAS-Flp*
S4	A	*w^{1118}*
	B	*w;; fat2$^{\Delta ICD}$-3xGFP, FRT80*
	C	*w^{1118}* *w;; fat2^{N103-2}, FRT80* *w;; fat2$^{\Delta ICD}$-3xGFP, FRT80/+* *w;; fat2$^{\Delta ICD}$-3xGFP, FRT80*
	D-F	*e22c-Gal4, UAS-Flp/+; fat2$^{\Delta ICD}$-3xGFP, FRT80/ubi-eGFP, FRT80*
	G	*w;; fat2$^{\Delta ICD}$-3xGFP, FRT80*
	H	*w^{1118}*
	I	*w;; fat2^{N103-2}, FRT80*
	J	*w;; fat2$^{\Delta ICD}$-3xGFP, FRT80*
S5	A	*w;; fat2-3xGFP, FRT80*
	B	*Lar^{bola1}/Lar^{bola2}; fat2-3xGFP, FRT80/+*
	C	*w;; fat2-3xGFP, FRT80*
	D	*w;; fat2^{N103-2}, FRT80*
	E	*w;; fat2$^{\Delta ICD}$-3xGFP, FRT80*
	F	*Lar^{bola1}/Lar^{bola2}; fat2-3xGFP, FRT80/+*
S6	A	*e22c-Gal4, UAS-Flp/+; ubi-eGFP, FRT80/FRT80*
	B	*e22c-Gal4, UAS-Flp/+; fat2^{N103-2} FRT80/ubi-eGFP, FRT80*
	C	*SCAR^{k13811}, FRT40/ubi-eGFP, FRT40; T155-Gal4, UAS-Flp/+*
	D	*e22c-Gal4, UAS-Flp/+; fat2$^{\Delta ICD}$-3xGFP, FRT80/ubi-eGFP, FRT80*
	E	*e22c-Gal4, UAS-Flp/+; ubi-eGFP, FRT80/FRT80* *hsFlp/+;; Act5c>>Gal4, UAS-RFP/UAS-fat2-RNAi$^{TRiP.HMS02136}$* *e22c-Gal4, UAS-Flp/+; fat2^{N103-2} FRT80/ubi-eGFP, FRT80* *e22c-Gal4, UAS-Flp/+; fat2$^{\Delta ICD}$-3xGFP, FRT80/ubi-eGFP, FRT80* *Lar$^{13.2}$, FRT40/ubi-mRFP-nls, FRT40; T155-Gal4, UAS-Flp/+* *SCAR^{k13811}, FRT40/ubi-eGFP, FRT40; T155-Gal4, UAS-Flp/+*
	F	*Lar$^{13.2}$, FRT40/ubi-mRFP-nls, FRT40; T155-Gal4, UAS-Flp/+*
S7	A	*e22c-Gal4, UAS-Flp/+; msn-YFP, FRT80/FRT80*
	B	*e22c-Gal4, UAS-Flp/+; msn-YFP, fat2^{N103-2}, FRT80/FRT80*
	C, D	*hsFlp/+;; Act5c>>Gal4, UAS-GFP/UAS-CLASP-RNAi$^{TRiP.HMS01146}$*
	E	*sqh-GFP*
	F	*sqh-GFP, fat2^{N103-2}, FRT80/FRT80*
	G	*sqh-GFP* *sqh-GFP, fat2^{N103-2}, FRT80/FRT80*